



The Abdus Salam
International Centre for Theoretical Physics


United Nations
Educational, Scientific
and Cultural Organization


International Atomic
Energy Agency



SMR.1676 - 32

8th Workshop on Non-Linear Dynamics and Earthquake Prediction

3 - 15 October, 2005

Block structure modeling of dynamics and seismicity in the Italian area and surroundings

Inessa Vorobieva
Russian Academy of Sciences
International Inst. of Earthquake Prediction Theory and
Mathematical Geophysics
Warshavskoye Sh. 79. Kor2
117556 Moscow
Russia

These are preliminary lecture notes, intended only for distribution to participants

*Block structure modeling of dynamics and seismicity in the
Italian area and surroundings*

A. Peresan¹, I. Vorobieva², A. Soloviev^{2,3}, G.F. Panza^{1,3}

¹Department of Earth Sciences, University of Trieste, via E. Weiss 1, 34127
Trieste, Italy.

²International Institute of Earthquake Prediction Theory and
Mathematical Geophysics.
Russian Academy of Sciences. Warshavskoe sh.79, kor.2, Moscow 113556,
Russia.

³The Abdus Salam International Centre for Theoretical Physics - SAND
Group
ICTP, 34100 Trieste, Miramare, Italy.

Abstract

The block model of the lithosphere structure is used to simulate the dynamics and seismicity in the Italian region. The region is represented as a system of perfectly rigid blocks, separated by infinitely thin fault planes, in viscoelastic interaction between themselves and with the underlying medium. The movement of the boundary blocks and of the underlying medium determines the motion of the blocks. The purpose of the study is to understand: what are the tectonic processes that control the kinematics of the region and the main features of the observed seismicity. The influence of the rheology of the fault systems has been studied as well. The counter-clockwise rotation of the Adria is mimed; the model correctly reproduces the extension zone along the Apennines and the contraction zone along the north-western boundary of the Adriatic Sea. The movements of the blocks are in agreement with GPS (Global Positioning System) observations, and the synthetic seismicity is similar to the observed one for the most seismically active areas. Linear frequency-magnitude (FM) relation (Gutenberg-Richter law) is obtained for synthetic seismicity; the slope (b -value) of FM plot appears larger for the synthetic seismicity than for the observed one. Nevertheless, the b -value is essentially larger in Northern and Central Italy than that in Southern Italy, both in the model and in the observations. The analysis of the source mechanisms of the synthetic earthquakes shows a good agreement with the observations. In the model, normal faulting is typical for the Apennines, the eastern edge of Sicily and the Calabrian arc, while reverse faulting takes place at the north-western boundary of the Adriatic Sea, in the Southern Alps and along the Eastern edge of the Adria, along the Dinarides. The results of the modeling show that the main features of dynamics and seismicity in the Central Mediterranean region cannot be satisfactorily explained as a consequence of Africa and Eurasia convergence only; the passive subduction in the Calabrian arc and the different rheology of faults are essential as well.

Key words: Block model; lithosphere dynamics; numerical simulation; seismicity; synthetic catalog; Italy.

1. Introduction

Earthquakes occur as a result of different processes, which are still not entirely described and understood. A possible approach to overcome the difficulties in studying seismicity that are caused by the absence of fundamental constitutive equations for the dynamics of the lithosphere and the impossibility of direct measurements at depth, where the earthquakes originate, relies on the integration of the numerical modeling of the lithosphere dynamics with the phenomenology of earthquake occurrence.

A number of dynamical models have been proposed to simulate seismicity, the most popular being the spring-slider block model of Burridge and Knopoff (1967). Some models are "non-Earth specific" and reproduce only the very general features of seismicity, such as the frequency-magnitude relation. Some other try to simulate, at the cost of additional assumptions, further properties of the seismic sequences, like fluctuations in the activity and the space distribution of events (e.g., Yamashita and Knopoff, 1992). Each model tries to reproduce some peculiar properties of seismicity, based on different dynamical, kinematical or geometrical assumptions; nevertheless, no model can be expected to describe exactly the evolution of the Earth system, due to its complexity and possibly chaotic behavior.

Another type of numerical models that have been proposed so far is focused on the study of geodynamics. Among the studies devoted to the Mediterranean region, Bassi and Sabadini

(1994) and Bassi et al. (1997) showed, by means of a thin-sheet viscous model, that the subduction of the Ionian lithosphere underneath the Calabrian arc is necessary to explain the extensional style of the Tyrrhenian sea, while Negredo et al. (1999) showed the effect of three-dimensional subduction structures in controlling the retreat velocity along the hinge of the subduction. A number of studies, based on the viscous thin-sheet model (Cianetti et al., 1997) and on two-dimensional elastic thin-shell modeling (Meijer and Wortel, 1996; Lundgren et al., 1998) are concentrated on the kinematics and stress patterns in the Aegean region. In particular, Giunchi et al. (1996) studied, in the Aegean Sea, the effects of the relative plate velocities on the stress pattern and showed that it has a major influence on the earthquake distribution with depth. Recently, Jimenez-Munt et al. (2003) used the thin-shell finite element approach to simulate active deformation in the Mediterranean region. This model, which permits to simulate the effects of the negatively buoyant density contrasts of the subducted lithosphere, on the horizontal velocity at the surface, evidenced that the deformational style in the Mediterranean region is controlled by the Africa-Eurasia convergence and by the subduction in the Calabrian Arc and Aegean Sea. Finally, Battaglia et al. (2004) use GPS and block modeling (Murray and Segall, 2001) to investigate present day deformation of Adriatic region, and they compute rigid-plate angular velocities while accounting for elastic strain accumulation along block-bounding faults. The method they use, proposed by Murray and Segall (2001), differs from the block structure dynamics simulation introduced by Gabrielov et al. (1990) and that we use here. Battaglia et al. (2004) argue that the Adria behaves as an independent microplate, its southern boundary with the Nubia (Africa) plate being located along the Apulia escarpment and the Keffalina fault. The best agreement between GPS observations and modeled velocities is predicted when the Adria is divided into two subplates along the Gargano-Dubrovnik fault, in agreement with the kinematical models of Benedetti (1999), the complex geodynamic evolution of the Balkan area (Pamic et al., 2002) and recent tomographic studies (Venisti et al., 2004).

The numerical models mentioned above give possibility to study geodynamics of a region under consideration. Using these models one can predict velocities, slip rates, stresses and some other physical parameters and try to reconstruct the geological history of the region. But these models do not simulate seismicity and therefore cannot be used for studying seismicity dependence on geodynamics. The model of the lithosphere block structure dynamics considered in this paper, aims to the simultaneous study of both geodynamics and seismicity for a given region. This is made possible by introducing simplifications. The basic one is an assumption that the blocks are perfectly rigid. This assumption is justified by the fact that in the lithosphere the effective elastic moduli of the fault zones are significantly smaller than the ones within the blocks and it is rather realistic for short (as compared with the geological history) periods of simulation (thousands of years). The method allows us to use a realistic geometry of the blocks, based on any relevant information. Driving tectonic forces (velocities of the boundary blocks and underlying medium) can be prescribed using geodetic data (GPS, VLBI), and the rheology of fault zones (parameters reflecting elasticity and viscosity) can be taken into account, as well, using the knowledge about the lithosphere structure, in terms of geometries and velocities of seismic waves propagation, and heat flow data.

The model simulates both fast (synthetic seismicity) and slow (tectonic motions) movements of blocks, and it provides a straightforward tool for a broad range of problems, like: (i) connection between seismicity and geodynamics; (ii) dependence of seismicity on the general properties of the fault networks and rheology; (iii) formulation and testing of different hypothesis for earthquake forecasting purposes.

The model, described in detail by Soloviev and Ismail-Zadeh (2003), considers a seismic region as a system of blocks divided by infinitely thin plane faults. The blocks are assumed to be perfectly rigid. The interaction of the blocks between themselves and with the underlying medium is visco-elastic. The system of blocks moves as a consequence of the motions prescribed for the boundary blocks and for the underlying medium. As the blocks are perfectly rigid, all the deformations take place in the fault zones and between the blocks and the underlying medium.

The interaction of blocks along the fault zones is viscoelastic ("normal state"), until the ratio of the shear stress to the normal one remains below a certain strength level. When the critical strength level is exceeded in some part of a fault zone, a stress-drop ("earthquake") occurs. The earthquake is defined as an abrupt change of the inelastic displacement.

It might be argued that continental deformation should be described by a velocity field, rather than by the relative motions of rigid blocks. But a velocity field that describes the average deformation is only a partial description of what is happening because it does not describe the detailed discontinuous deformation of the seismogenic layer (Jackson, 2003). In the block model the movement of blocks, which corresponds to a velocity field "discretized" at the scale of blocks, is reproduced as a result of modeling.

The output of the modeling consists of kinematical data on the block movements, that can be compared with observations (e.g. GPS), as well as of a synthetic earthquake catalog, where each event has origin time, coordinates of epicenter, magnitude and source mechanism. On the basis of the experience accumulated so far, the synthetic earthquake catalog reproduces not only some of the basic global features of observed seismicity like (a) the Gutenberg-Richter law (e.g., Panza et al., 1997), (b) the space and time clustering of earthquakes (Maksimov and Soloviev, 1999) and (c) the dependence of the occurrence of large earthquakes on the fragmentation of the faults network, and on the rotation of blocks (Keilis-Borok et al., 1997), but also several regional features of seismicity, like (1) the epicenter distribution, (2) the relative level of seismic activity in different areas of the region and (3) the type of fault plane solution.

The geometry of real faults and blocks has been first considered in the block model of the Vrancea (Romania) earthquake-prone region (Panza et al., 1997). A set of numerical experiments, performed adjusting the model parameters, permitted to obtain a spatial distribution of synthetic epicenters close to that observed in the Vrancea region. Assuming this set of parameters as a benchmark, the dependence of the features of the synthetic catalog on the model's parameters has been subsequently investigated (Soloviev et al., 1999). The source mechanisms of the largest synthetic earthquakes, defined by the slip angles along the given faults, resulted to be close to the average ones observed for the large earthquakes that occurred in the Vrancea subduction zone (Soloviev et al., 2000). The effect, on the intermediate-depth seismicity, of a sinking relic slab beneath Vrancea has been studied, as well by means of the model of the block structure dynamics (Ismail-Zadeh et al., 1999). Changes in synthetic seismicity, due to small variations in the slab rotation, are in overall agreement with the hypothesis of Press and Allen (1995) that small changes in the direction of the plate motion control the pattern of seismic release. The results of these experiments have shown that the similarity between the features of synthetic and observed seismicity can be used as a criterion to define, by a "trial-and-error" process, the range of parameters characterizing the tectonics of a given region. In particular, it seems possible to use the procedure of the block-structure dynamics modeling for the reconstruction of the different directions of the tectonic motion.

The block model of the Sunda Arc has been used to study the dependence of synthetic seismicity features on the specified movements. Soloviev and Ismail-Zadeh (2003) showed that the main features of synthetic seismicity are close to observations when the movement of Australia relative to Eurasia is specified in accordance with HS2-NUVEL-1 model (Gripp and Gordon, 1990). The common features are the locations of the larger events, the direction of migration of earthquakes, and the b -value of the Gutenberg-Richter law.

The block model of the Western Alps (Vorobieva et al., 2000; Soloviev and Ismail-Zadeh, 2003) has been developed on the basis of the morphostructural scheme due to Cisternas et al. (1985). The space distribution of epicenters of synthetic earthquakes reflects some features of the observed seismicity distribution. Gutenberg-Richter laws for the synthetic and observed seismicity are similar.

In this study, we consider a region covering Italy and surroundings. The block structure has been outlined on the basis of the seismotectonic model developed by Meletti et al. (2000), and the space distribution of seismicity. The idea to represent this region as a system of perfectly

rigid blocks is supported by the existence of some large, almost aseismic territories, like the Adria micro-plate. The area of active deformation along the Apennines, in the present study, is simplified: Apennines are represented by two blocks bounded by parallel system of faults, which are assumed to represent as a whole the complex system of small faults. The purpose of the study is to understand what tectonic processes control the kinematics of the region and the features of the observed seismicity, as well as the influence of the rheology of the fault system on the seismicity. To estimate the quality of the modeling, the results of the numerical simulation are compared with the observations. Specifically, the block motions are checked against geodetic observations (GPS and VLBI), while the epicenter distribution, the location of the largest events, the type of source mechanisms and the slope of the Gutenberg-Richter law for the synthetic seismicity are compared with the observed ones.

2. Brief description of the model

A block-structure is a limited and simply connected part of a layer, d , with thickness H , bounded by two horizontal planes (Figure 1). The portions of planes intersecting the layer, called "fault planes", form the lateral boundaries of the block-structure and its subdivision into blocks. The intersection lines of the fault planes with the upper plane are called "the faults". The fault planes can have arbitrary dip angles, which are specified on the basis of information on the lithospheric structure of the region under consideration. A common point of two faults is called "vertex". The vertices on the upper and the lower planes are connected by a segment ("rib") of the intersection line of the corresponding fault planes (see Figure 1). The upper and the lower surfaces of the blocks are polygons. The lower surface of the block is called "the bottom". The topology of the fault structures in the upper and lower planes is the same. The block-structure is bordered by a confining medium. The motion of the confining medium is defined in the continuous parts, delimited by two ribs of the block structure boundary, called "boundary blocks". The blocks are assumed to be rigid, and their relative displacements take place along the fault planes. The interaction of the blocks with the underlying medium takes place along the lower plane, any kind of slip being possible. The fault planes and the bottoms of the blocks are assumed to be infinitely thin viscous-elastic layers.

The movements of the boundary blocks and of the underlying medium are assumed to be due to the external forces. The rates of these movements are assumed to be horizontal and known. The movement rates of the underlying medium and of the boundary blocks can be different for each block.

Dimensionless time is used in the model. All variables containing time are referred to one unit of the dimensionless time, and the real time corresponding to the unit of the dimensionless time can be estimated at the interpretation stage of the results.

Elastic forces arise in the lower plane and in the fault planes as a result of the displacement of the blocks relative to the underlying medium, to the lateral boundary, and to the other blocks. The elastic stress (the force per unit area) at a point is proportional to the difference between the relative displacement and the slippage (the inelastic displacement) at the point. The rate of the inelastic displacement is proportional to the elastic stress. Accordingly,

$$\mathbf{f} = K(\Delta\mathbf{r} - \delta\mathbf{r}), \quad \frac{d\delta\mathbf{r}}{dt} = W\mathbf{f}, \quad (1)$$

where \mathbf{f} is the shear stress vector (elastic force per unit area acting along the fault plane or the block base) at the point of the lower plane or of the fault plane, $\Delta\mathbf{r}$ is the vector representing the relative displacement, and $\delta\mathbf{r}$ is the vector representing the inelastic displacement. Equations (1) correspond to visco-elastic (Maxwell) rheological law that describes the relation of \mathbf{f} to the strain ζ

$$\left(\frac{d}{dt} + \frac{1}{\tau} \right) \mathbf{f} = \mu \frac{d\zeta}{dt} \quad (2)$$

where τ is the relaxation time ($\tau = \eta / \mu$), μ is the shear modulus, and η is the viscosity. Coefficients in (1) and (2) are connected by formulas: $K = \mu/a$, $W = a/\eta$, where a is the actual width of the fault zone and $\tau = 1/(KW)$.

On the fault plane, the reaction force is normal to the fault plane and its size, per unit area, is:

$$|p_0| = |f_1 \operatorname{tg} \alpha| \quad (3)$$

where f_1 is the component of the elastic stress, \mathbf{f} , normal to the fault on the upper plane, and α is the dip angle of the fault plane. The value of p_0 is positive in the case of extension and negative in the case of contraction, respectively.

The displacements of the blocks are described by the components of their translation vectors and the angles of their rotation around the geometrical centers and are supposed to be infinitely small, compared with the block size. Therefore the geometry of the block structure does not change during the simulation and the structure does not move as a whole.

At each time moment the displacements of the blocks are found from the condition that the total force and the total moment of forces acting on each block are equal to zero. This is the condition of quasi-static equilibrium of the system and, at the same time, the condition of minimum energy. The equilibrium equations include only forces caused by the specified movements of the underlying medium and the boundaries of the block structure. In fact, it is assumed that the action of all other forces (gravity, etc.) on the block structure is ruled out and does not cause displacements of blocks.

The state of the block structure is considered at discrete values of time $t_i = t_0 + i\Delta t$ ($i = 1, 2, \dots$), where t_0 is the initial time. The transition from the state at t_i to the state at t_{i+1} proceeds as follows: (i) new values of the inelastic displacements are calculated accordingly to equations (1); (ii) translation vectors and rotation angles at t_{i+1} are obtained for boundary blocks and the underlying medium; (iii) the translation vectors and the angles of rotation for the blocks are determined from the equilibrium equations.

The space discretization, that is necessary to carry out the numerical simulation of block structure dynamics, is made by splitting the surfaces (fault planes and block bottoms), on which the forces act, into cells with linear size not exceeding a parameter ϵ . The coordinates X, Y , the relative displacement $\Delta \mathbf{r}$, the inelastic displacement $\delta \mathbf{r}$, and the elastic stress \mathbf{f} are supposed to be the same for all the points of a cell.

The earthquakes are simulated in accordance with the dry friction model. For each cell of the fault planes, the quantity

$$\kappa = \frac{|\mathbf{f}|}{P - p_0} \quad (4)$$

is introduced, where \mathbf{f} is given by (1), P is a parameter of the model which is assumed to be equal for all the faults. P can be interpreted as the difference between the lithostatic (due to gravity) and the hydrostatic pressure, which is assumed to be equal to 2 Kbars for all the faults, and p_0 is the reaction force per unit area, given by (3).

Three following values of κ are assigned for each fault:

$$B > H_f \geq H_s.$$

It is assumed that the initial conditions of the model satisfy the inequality $\kappa < B$ for all cells of the fault planes.

If, at some time t_i , the value of κ in any cell of a fault plane reaches the level B ($\kappa \geq B$), a failure ("earthquake") occurs. The failure is considered slippage during which the inelastic displacement $\delta \mathbf{r}$ in this cell changes abruptly to reduce the value of κ to the level H_f . The new - after the failure - vector of the inelastic displacement $\delta \mathbf{r}^e$ is calculated from

$$\delta \mathbf{r}^e = \delta \mathbf{r} + \delta \mathbf{u}, \quad \delta \mathbf{u} = \gamma \mathbf{f} \quad (5)$$

where $\delta \mathbf{r}$ and \mathbf{f} are the inelastic displacement and the elastic stress, defined by (1), just before the failure and the coefficient γ is determined from the condition that $\kappa = H_f$ after the failure. Once

the new values of the inelastic displacements for all the failed cells are computed, the translation vectors and the angles of rotation of the blocks are determined to satisfy the condition of quasi-static equilibrium. If after these computations, for some cell(s) of the fault planes still $\kappa > B$, the procedure is repeated for this (these) cell(s), otherwise the numerical simulation is continued in the ordinary way.

On the same fault plane, the cells in which failure occurs simultaneously form a single earthquake. The coordinates of the earthquake epicenter are determined as the weighted sum, with weights proportional to the areas of the failed cells, of the coordinates of the cells forming the earthquake. The magnitude of the earthquake is calculated from Utsu and Seki, (1954):

$$M = 0.98 \log_{10} S + 3.93 \quad (6)$$

where S is the total area of the cells forming the earthquake, measured in km^2 .

For each earthquake, the source mechanism can be determined considering the vector $\Delta\mathbf{U}$, defined as the weighted sum, with weights proportional to the areas of the failed cells, of the vectors $\delta\mathbf{u}$, given by (4), for the cells forming the earthquake. From (1) and (4) it follows that $\Delta\mathbf{U}$ lies in the fault plane where the earthquake occurs.

Immediately after each earthquake, it is assumed that the cells in which the failure occurred are in the creep state. It means that, for these cells, in equation (1), which describes the evolution of the inelastic displacement, the parameter W_s ($W_s > W$) is used instead of W . After the earthquake, the cell is in the creep state as long as $\kappa > H_s$, when $\kappa \leq H_s$, the cell returns to the normal state and henceforth the parameter W is used in (1) for this cell.

3. Geodynamics and block structure for the Italian region and its surroundings

Different criteria can be followed to define the geometry of the block structure, which depends from the main geological elements of the region as well as the scale and detail of the model. In some previous studies the morphostructural zonation of the study region, e.g. the Western Alps, has been used (Vorobieva et al., 2000; Soloviev and Ismail-Zadeh, 2003) as the base for the block structure geometry. In the present work that is performed on a larger space scale we use as a base the seismotectonic model of the study area (Scandone et al., 1990, 1994, Meletti et al., 2000)

According to Meletti et al. (1995, 2000), the recent geodynamics of the Central Mediterranean region is controlled by the Africa-Europe plate interaction and by the passive subduction of the south-western margin of the Adria plate. The main regional geological features observed in Italy and surroundings (Figure 2) are represented by the Alps, by the back-arc Tyrrhenian extensional basin, by the Apennines and by the Padan-Adriatic-Ionic foreland. The Ortona-Roccamonfina line (Scandone et al., 1990) connects two major arcs in the Apennines chain corresponding to the north-central and southern Apennines. The extensional rate that characterizes the southern part of the Tyrrhenian basin exceeds considerably those observed in the northern part. The boundary between these parts lies nearby the 41°N parallel and it is associated with a discontinuity, marked by magnetic anomalies.

Apennines, Alps and Dinarides outline the western, northern and eastern boundaries of the Adria respectively, while the location of the southern boundary is controversial. A counter-clockwise rotation of the Adria justifies the main characteristics, both structural and kinematics, of its boundary regions (Anderson and Jackson, 1987; Ward, 1994), such as the contraction front extending along the northeastern boundaries of the plate and its indentation in the Western Alps. Passing from east to west the structural features change: the Adria is subducting under the Eastern Alps and the Apennines, while in the Western Alps it is overthrusting the European plate (Meletti et al., 1995; Schmid et al., 1996). Therefore the boundary between the Alps and the Apennines is a transform fault zone connecting the opposite lithospheric sinking. The evolution of the Apennines, however, does not seem to be explained by a simple convergence process and some evidences suggest that it may be controlled mainly by passive subduction processes (Meletti et al., 1995; Pasquale et al., 1997; Doglioni, 1991; Doglioni et al., 1999a).

A band with tensional seismotectonic behavior, with prevailing dip-slip focal mechanism, characterizes the northern part of the Italian peninsula, from the Po plain to the Ortona-Roccamonfina line. Two belts run parallel to it: the western one is composed by the tensile zones near to the Tyrrhenian coast and the eastern one by the contraction zones along the Adriatic Sea. The model proposed by Meletti et al. (2000) for the deep structure of the north-central Apennines includes a connection at depth between the Adriatic contraction front and the uplifting asthenosphere along the Tyrrhenian Sea. This agrees with the geometry of the lithosphere-asthenosphere system outlined by Calcagnile and Panza (1981), Panza et al. (1982), Della Vedova et al. (1991), Marson et al. (1995) and refined very recently by Chimera et al. (2003) on the basis of relevant geophysical observations (surface waves and body waves tomography, heat flow, gravity).

The passive subduction of the Adriatic foreland in the Southern Apenninic Arc, from the Ortona-Roccamonfina line to the Taranto Gulf, may be ceased due to a tear apart in the subducted slab, while it continues in the concave part of the Calabrian Arc, where a zone of active seismicity is identified, emerging toward the Tyrrhenian basin and reaching a depth of about 500 km (Caputo et al., 1970, 1972; Anderson and Jackson, 1987; Panza et al., 2003).

As concerning the Adria plate, it remains still undecided if it is connected to the Africa plate or if it moves as an independent plate, since neither a structural nor a seismically active boundary between the Adria and Africa plate is clearly evidenced (Panza, 1984). At the same time the stress distribution appears compatible with a counter-clockwise rotation of the Adria, with respect to Eurasia, whose rotation pole is well distinguished from that proposed for the Africa-Eurasia rotation. Therefore the movement of the Africa plate appears different from the motion of its old promontory. The lithospheric heterogeneities recently outlined by Venisti et al. (2004) seem to corroborate the fragmentation of the Adriatic plate, as required by the kinematics models of Benedetti (1999), the dynamic models by Battaglia et al. (2004), and the complex geodynamic evolution of the Balkan area (Pamic et al., 2002).

Summing up, the available information is not sufficient to define the block structure of the region in a unique way. Taking as the basis the structural sketch shown in Figure 2 (Meletti et al., 2000) and the main features just discussed, we have outlined the block structure designed for modeling dynamics and seismicity of the region. The configuration of its faults, on the upper plane, is shown in Figure 3. The fault locations take into account the seismotectonic model of Italy (Scandone et al., 1994; Meletti et al., 2000) and the distribution of the observed seismicity within the outlined block structure (Figure 4). In fact, since one of the aims of the model is to reproduce the main features of the space distribution of observed seismicity, the modeled faults have to be introduced in the structure corresponding to the most seismically active areas and fault zones.

The complex geodynamics of the studied region requires the consideration of an adequately complex block structure, capable to model a structure dynamic representative of the real one. Several parameters, describing its dynamical properties, must be defined for each block; hence the limited availability of observations, about the real motion of the structure, imposes limitations on the amount of details that can be introduced in the block structure (e.g. smallest block size).

The block structure (Figure 3) consists of eleven blocks. These blocks are contoured by 36 faults. The point with the geographic coordinates 43.0°N and 13.0°E is chosen as the origin of the reference coordinate system. The X-axis is the east-oriented parallel passing through the origin of the coordinate system and the Y-axis is the north-oriented meridian passing through the origin of the coordinate system. The blocks and the faults composing the structure are marked in Figure 3 from I to XI and from 1 to 36, respectively.

Two main longitudinal discontinuities (faults 25 - 29) have been placed along the North-Central Apennines, to model the Adriatic contraction front and the extension belt. Fault 8 has been placed, corresponding to the Ortona-Roccamonfina line (Meletti et al., 2000), while faults 30 and 32 have been placed south of it to model the seismic activity from Irpinia to the Pollino,

along the Southern Apennines. A possible discontinuity (fault 11) is assumed to exist between Adria and Africa plates, south of Apulia; an almost EW oriented discontinuity (fault 33) has been placed according to the observed seismicity, crossing the Gargano and the Adria plate from the Apenninic chain up to the Dinarides. Battaglia et al. (2004) also assume a similar boundary, dividing Adria into two subplates separated by the Gargano-Dubrovnik fault, in agreement with the parametric studies by Oldow et al. (2002). Nine boundary blocks, which are marked as BB1 - BB9 in Figure 3, are introduced to specify the motion of the confining medium at the lateral boundaries of the structure.

To choose the value of the thickness H of the layer d we analyze the distribution of the hypocenters of observed seismicity. Most of them are within 30 km depth. Another reason to specify $H = 30$ km is given by the new data on the deep structure of Italy and surroundings. According to Chimera et al. (2003) and Panza et al. (2003) there is a rather large lithospheric zone, at an average depth of about 30km, where the S-wave velocity is rather low. This mantle wedge is a generalized feature, identified in the uppermost mantle along the Apennines and the Calabrian Arc, and it underlies all the recent volcanoes. Therefore partial melting can be relevant in this part of the uppermost mantle, and it is reasonable to assume that this is a zone of increased plasticity, where lithospheric delamination occurs, with consequent decoupling between the upper and lower layers of the lithospheric mantle.

The dip angles of the faults have been specified on the basis of the source mechanisms of the observed earthquakes given in Figure 5 (Sarao' et al., 1997). The faults have been separated into two groups: near-vertical and oblique faults. The same value of the dip angle has been assigned to all the faults belonging to the same group: 85° - for near-vertical faults, and 60° - for oblique faults. The dip angle of each fault is indicated in Figure 3.

The results of recent geodynamical reconstructions for the central Mediterranean area have been considered, including GPS measurements (Anzidei et al., 1996, Devoti et al., 2002), VLBI (Ward, 1994) and paleomagnetic evidences (Sagnotti, 1992; Sagnotti et al., 1994; Aifa et al., 1988). The directions of the most compressive horizontal principal stress from the World Stress Map (Mueller et al., 2000) and the map of active stress for the Italian region (Montone et al., 1999) have been taken into account as well. This information has been used to choose the prescribed velocities of the boundary blocks and underlying medium.

A problem that we encounter in defining the model is the adequate representation, using a bidimensional system of absolutely rigid blocks, of the opening of the Tyrrhenian basin and of the passive subduction of the Ionian-Adria lithosphere, with the consequent flexure axis retreat. To reduce the problem to two dimensions we make the following assumption. The extension due to the uprising mantle flow is modeled by displacements of blocks that can be obtained by means of a pulling force, applied by the boundary blocks and block bottoms (Buck, 2003), while contraction can be described by means of a pushing force (see Figure 6). This way we model non-horizontal driving forces and movements in the fault planes, applying equivalent horizontal driving motions. A similar task of reducing a three-dimensional problem to two dimensions has been considered by Jimenez-Munt et al. (2003), where vertical forces have been reduced to their horizontal equivalents (e.g. trench suction in the Calabrian Arc).

The block structure thus defined and the above mentioned information have been the starting point for a wide set of numerical experiments described below, which permitted, step by step, to reproduce several relevant features of the observed kinematics and seismicity.

4. Numerical Experiments

The values of the parameters for the blocks and the faults and the movements specified for the underlying medium and the boundary blocks have been varied in a set of parametric experiments. We report here about the six experiments that we consider more significant. The following set of values has been assumed as a benchmark and we call it, from now on, the "standard set".

For all blocks and faults the coefficients in (1) are: $K = 1$ bar/cm and $W = 0.05$ cm/bar. For all faults the thresholds for κ are: $B = 0.1$, $H_f = 0.085$, and $H_s = 0.07$, and for $W_s = 5$ cm/bar, like those used in previous studies (i.e. Panza et al., 1997; Soloviev et al., 2000; Vorobieva et al., 2000). These parameters reflect the rheology of fault zones, but a specific analysis to estimate how they correspond to specific publications on this subject (see, e.g., Karner et al., 2004) goes beyond the scope of the present study. The medium underlying all the blocks, and the boundary blocks BB1 - BB3 and BB6 - BB9 do not move. The boundary blocks BB4 and BB5 move progressively with the velocity $V_x = -25$ cm, $V_y = 65$ cm per unit of dimensionless time, respectively. This direction of velocity has been chosen accordingly to NUVEL-1A model (Gripp and Gordon, 1990; DeMets et al., 1990; DeMets et al., 1994). In all experiments the value of P in (4) equals 2 Kbars, and the values of the parameters for the discretization, in time and space, are $\Delta t = 0.0001$ and $\varepsilon = 5$ km, respectively.

The movements of the underlying medium and of the boundary blocks have been specified in the experiments taking into account the following main features of the geodynamics of the region:

- convergence of African and European plates;
- counterclockwise rotation of the Adria plate, with the pole of rotation in the Western Alps;
- opening of the Tyrrhenian basin.

The following features of the observed seismicity, which follow from the analysis of the epicenter distribution and source mechanism, have been used to estimate the results of the experiments:

- two seismoactive belts in the north-central Apennines: the eastern one in contraction, the western one in extension;
- double extensional belt in the Southern Apennines;
- contractional belts along the Dinarides and the Southern Alps;
- absence of seismicity along the southern boundary of the structure, i.e. unknown boundary between Africa and Adria.

We should note that the number of free parameters in the model is rather high. They include 6 parameters (K , W , W_s , B , H_f , and H_s) for each of 36 faults, 5 parameters (K , W , V_x , V_y , and the angle velocity of rotation) for each of 11 block bottoms, 3 parameters (V_x , V_y , and the angle velocity of rotation) for each of 9 boundary blocks, and 4 general parameters (H , P , ε , and Δt). Therefore the total number of free parameters is 302. But parameters P , ε , Δt , K , B , H_f , and H_s are not changed in our numerical experiments, when changing values of W and W_s we keep relation $W_s = 100W$, and zero angle velocity of rotation is specified for all block bottoms and boundary blocks. This reduces the total number of free parameters to 88. But actually we changed in the experiments described below the values of 33 parameters only.

A qualitative comparison the modeling results with observed seismicity and geodynamics is made in the first steps of the study (Experiments 1-5 below). The quantitative comparison is made in the final step (Experiment 6) when qualitative agreement with the observation is obtained.

Experiment 1

Purpose: to check, if the convergence of Africa and Europe alone can explain the main features of tectonics and seismicity in the region.

Values of the parameters: the standard set given in Section 3.

Result. Adria undergoes a counterclockwise rotation, but its northern part (block IV) moves NW, and not North, as it should be to reproduce observations (Nocquet and Calais, 2003). Most of the synthetic seismicity is concentrated along the southern boundary of the structure where the observed seismicity is absent. Excluding two clusters of events in the Alps, the synthetic seismicity is absent in the northern part of the model where, on the contrary, the observed seismicity is considerable. The displacements of the blocks are listed in Table 1, and the epicenters of the synthetic earthquakes are shown in Figure 7.

Experiment 2

Purpose: to check, the dependence of the model behavior on the thickness of the structure.

Values of the parameters: the standard set, with exception for the value of H which is set to 15 km.

Result. The displacements of the blocks and the distribution of the epicenters of the synthetic earthquakes look like those obtained in Experiment 1, but the synthetic seismicity in the Alps disappears and the level of seismic activity decreases. The displacements of the blocks are listed in Table 2, and the epicenters of the synthetic earthquakes are shown in Figure 8.

Experiment 3

Purpose: to change the direction of motion of the northern part of the Adria (block IV), and to improve the fit with observed seismicity by removing the synthetic seismicity from the southern boundary of the block structure and by making seismically active its northern part.

Values of the parameters: The standard set is modified as follows. The translational velocities of the boundary block BB4 and of the underlying medium, for blocks IV - VIII and XI, correspond to a rotation of the Adria plate around the pole with geographical coordinates 44.2°N and 8.3°E (Meletti et al., 2000). This means that the prescribed velocities are orthogonal to the radius vector from the pole of rotation to the center of the block and that the values of the velocities are proportional to its distance from the pole of rotation (as given in table 3). These NE oriented velocities prescribed for the underlying medium account also for the probable global eastward drift of the asthenosphere relative to the lithosphere, as suggested by Doglioni et al. (1999b). No rotational components of velocity are prescribed. The velocity of the underlying medium for block X is the same as the velocity of the boundary block BB5, $V_x = -25$ cm, $V_y = 65$ cm. per unit of dimensionless time.

Result. A counterclockwise rotational component of the movement for blocks IV and VI, representing the Adria plate, is obtained. The northern part of the Adria (block IV) moves north. Extension along the double faults 30, 32 in the Southern Apennines and contraction along the Dinarides (faults 9, 10) are obtained, but the model does not reproduce the extension–contraction belt in the North-Central Apennines (faults 25 - 29). The southern boundary of the structure becomes aseismic, while the northern part of the structure is active till the Alps. High seismicity appears at the eastern edge of Sicily. The double seismic belt appears in the Southern Apennines, but there is no synthetic seismicity at the western edge of the North-Central Apennines. The level of seismicity is not high enough in the Calabrian arc and in the Dinarides. The displacements of the blocks are listed in Table 3, and the epicenters of the synthetic earthquakes are shown in Figure 9.

Experiment 4

Purpose: to reproduce the extension–contraction belt in the North-Central Apennines and to increase the level of seismic activity in the Calabrian arc.

Values of the parameters: with respect to the set of parameters considered in Experiment 3, the following changes are made: the velocities of the boundary block BB7 and of the underlying medium for block III are replaced respectively by $V_x = -30$ cm, $V_y = 30$ cm, and by $V_x = 55$ cm, $V_y = 45$ cm. per unit of dimensionless time.

Result. The counterclockwise rotation of the Adria plate, the extension in the southern Apennines and the contraction along the Dinarides are obtained. The extension–contraction belts in the north-central Apennines are obtained as well. The synthetic seismicity appears at the western edge of the northern Apennines but its level is comparatively too high. The synthetic seismicity increases in the Calabrian arc but it is comparatively too high at the eastern edge of Sicily. The displacements of the blocks are listed in Table 4 and the epicenters of the synthetic earthquakes are shown in Figure 10.

Experiment 5

Purpose: to study how the synthetic seismicity depends on the coupling of the blocks with the underlying medium.

Values of the parameters: with respect to Experiment 4, W is decreased for blocks I, III, V, VII, and XI to 0.005 cm/bar, and for block II to 0.015 cm/bar.

Result. The level of the synthetic seismicity increases slightly in the contraction belt of the North-Central Apennines and remains too high at the western edge of Sicily and in the extension belt of Northern Apennines. The displacements of the blocks are listed in Table 5, and the epicenters of the synthetic earthquakes are shown in Figure 11.

Experiment 6

Purpose: to decrease the synthetic seismicity in the extension belt of the northern Apennines and at the eastern edge of Sicily, and to increase it in the contraction belt of the north-central Apennines.

Values of the parameters: with respect to the set of parameters used in Experiment 5 the following changes have been made: for faults 25 - 27 (the eastern side of the north-central Apennines) the values of W and W_s are set equal to 0.005 and 0.5 cm/bar, respectively, and for faults 15, 28, and 29 (the eastern edge of Sicily and the western edge of Northern Apennines) the values of W and W_s are set equal to 0.5 and 50 cm/bar, respectively.

Result. The synthetic seismicity decreases at the western edge of the north-central Apennines and at the eastern edge of Sicily, while it increases in the southern Apennines. The displacements of the blocks are listed in Table 6, and the epicenters of the synthetic earthquakes are shown in Figure 12.

5. Discussion

The purpose of the experiments described in section 4 is to reproduce the main features of geodynamics and of observed seismicity in the Italian area. We tested various hypotheses by changing the input parameters of the model. The variation of the velocities of the boundary blocks and of the underlying medium (experiments 1-4) allows us to check the influence of different tectonic forces on the geodynamics and seismicity of the study area, while the variation of the parameters controlling the rheology of the fault zones and block bottoms (experiments 5 and 6) allows us to fit, with the synthetic seismicity, several relevant features of the observed one.

When only the movement of the boundary blocks representing the African plate is specified (Experiment 1), it is impossible to reproduce the directions of the block motions and the distribution of the synthetic epicenters like those known from the observations. Decreasing the thickness of the structure (Experiment 2) increases the difference between synthetic and observed seismicity.

In Experiment 3 we assume the existence of an additional factor influencing the overall movement in the region under study: the probable global westward drift of the lithosphere relative to the asthenosphere (or eastward drift of the asthenosphere relative to the lithosphere) as suggested by Doglioni et al, (1999b), who showed that the subduction zones surrounding the Adriatic plate is consistent with the existence of a mantle wedge (Panza et al., 2003). We introduce the movement of the Adria plate, simulating a rotation around the pole in the Western Alps (Meletti et al., 2000), with direction in agreement with the configuration of the mantle wedge proposed by Doglioni et al, (1999b). The resulting movements of the blocks and synthetic seismicity become more similar to the observations than in Experiment 1. This fact can be interpreted as a confirmation that the Adriatic plate is an independent microplate (Battaglia et al., 2004).

Experiment 4 is based on the assumption that the geodynamics of the region is controlled not only by the convergence of Africa and Eurasia, but also by the passive subduction of the

south-western margin of the Ionian-Adria plate, which causes the opening of the Tyrrhenian basin (e.g. Pasquale et al., 1997). This speculation is supported by the results of Jimenez-Munt et al. (2003) who, by means of an independent method and considering a different scale of investigation, could not obtain a satisfactory result for the geodynamics of the studied area, taking into account the convergence of Africa and Eurasia only. We model the opening of the Tyrrhenian in its northern part by specifying the movement of the underlying medium for block III (the north-central Apennines) with a velocity in the NE direction that allows us to obtain extension at the western edge of the Apennines and contraction at its eastern edge. One may interpret this as the existence of a rising mantle flow (Pasquale et al., 1997; Sobolev and Rundquist, 1998), which causes the complex structure in the northern Apennines (Meletti et al., 2000; Chimera et al., 2003). This assumption may be confirmed by the high heat flow here (Della Vedova et al., 1991; Pollack et al., 1993). By specifying the movement of boundary block BB7 we model the opening of the Tyrrhenian basin in its southern part and as a consequence of this choice the synthetic seismicity in the Calabrian arc increases. Even if the tectonic motions are reproduced in the model more accurately than in the previous experiments, and the likelihood of synthetic epicenters distribution is improved considerably, the comparative levels of the synthetic seismicity, in the different parts of the structure, are not in sufficient agreement with the observations.

In Experiment 5 we change the visco-elastic characteristics of the block bottoms in Calabria, Apennines and Alps, more specifically we decrease the value of W - the growth rate of the inelastic displacements for these block bottoms. This change increases the viscous drag between the block bottoms and the underlying medium and models the coupling along the Apennines, Alps and in Calabria, where lithospheric roots have been evidenced by Panza et al. (2003). With respect to the previous experiments, the increase of coupling increases the transmission, to the blocks of the structure, of the motion of the underlying medium, and, as a result, the synthetic seismicity increases in the contraction belt of the north-central Apennines and in the southern Apennines.

In Experiment 6 we change the parameters that define the visco-elastic characteristics of the faults along the eastern edge of Sicily (fault 15 in Fig. 3) and the western edge of the north-central Apennines (faults 28, 29 in Fig. 3). The level of the synthetic seismicity obtained along these faults with Experiment 5 is too high. The faults along the eastern edge of Sicily and the western edge of the northern Apennines are located in extensional zones and we assume that the Earth crust here is possibly softer and more plastic than in other parts of the region. This assumption is in accordance with the heat flow data (Pollack et al., 1993; Della Vedova et al., 2001) and with the lithospheric S-wave velocities, as reported by Panza et al. (2003) and it allows us to assume that a considerable part of stress is released through creep without earthquakes. We therefore increase the parameters W and W_s that control the increment rate of the inelastic displacements and that may decrease the level of the synthetic seismicity along the faults 15, 28, 29. On the contrary, we decrease W and W_s for the faults along the eastern edge of the north-central Apennines (faults 25, 26, 27), as the heat flow is low here (Pollack et al., 1993; Della Vedova et al., 2001). As a result the synthetic seismicity in the western edge of the north-central Apennines and in the eastern edge of Sicily decreases.

The sixth variant of the model qualitatively reproduces the basic features of the observed seismicity: mainly the epicenter distribution and the relative levels of seismicity in different parts of the region, and the tectonic motions in the study area. Therefore in the following we analyze quantitatively and discuss in detail the results of Experiment 6.

5.1 Block movements

The numerical simulation of the block structure dynamics has been performed for a period of 20 units of dimensionless time. The resulting displacements of the blocks are shown in Figure 13 by open arrows, while the black arrows indicate the motion inferred from the geodetic measurements (Devoti et al., 2002). Observed movements are available for the blocks III, IV, VI,

X, XI. The movements obtained in the model exhibit a good agreement with these observations. The values of the translation and rotation of the blocks of the structure are given in Table 6. All blocks move in the NE direction, except blocks I and X, which represent Western Alps and Sicily and move in the NW direction. The absolute values of displacement decrease going northward, and blocks I and II, representing the Alps, are almost motionless; this fact is in qualitative agreement with the results of Jimenez-Munt et al. (2003) and might be explained, to some extent, by the predominance, there, of vertical motions (Gubler et al., 1981; Geiger et al., 1986; Brockmann et al., 2001, Calais et al., 2000), which cannot be reproduced by the modeling.

The counter-clockwise rotation of blocks IV and VI is in good agreement with the rotation of the Adria plate (Meletti et al., 2000). Comparing the resulting displacements of the blocks (Table 6 and Fig. 13) it is possible to observe that there is extension on faults 28, 29 30 and 32 in Figure 3, which represent the extension zone along the Apennines, and compression at the eastern edge of block III, which represents the contraction band, along the Adriatic Sea, in the North-Central Apennines. Contraction zones are formed along the eastern edge of blocks IV and VI (the boundary between Adria and Dinarides), and along the southern boundary of the Alps (fault 24 in Fig. 3); while an extension zone is obtained in the Calabrian Arc (faults 19 and 20 in Fig. 3). These results are in agreement with the stress map of Italy (Montone et al., 1999) and with the World Stress Map (Mueller et al., 2000).

5.2 Synthetic seismicity

The distribution of the epicenters of the synthetic earthquakes is shown in Figure 12. The magnitudes of the synthetic earthquakes are between 5.2, the minimum magnitude allowed by the specified value of ε (5 km), and 7.6. The information about the observed events is represented by the available historical data listed by Leydecker (1991), for the Dinarides, and by the catalog UCI2001 (Peresan and Panza, 2002) for Italy and its surroundings. The catalog UCI2001 is complete for magnitude 5 and above during the whole time interval 1000 – 2000, while the Leydecker catalog is complete in this range of magnitude only since 1900, but still very useful to identify where large earthquakes occurred during the last 1000 years in the part of the study area not covered by UCI2001.

There is a rather good agreement between the distributions of synthetic (Fig. 12) and observed (Fig. 4) epicenters. The slope (*b*-value) of the frequency-magnitude (FM) plot (Fig. 14), or Gutenberg-Richter law, appears larger for the synthetic seismicity (1.44 ± 0.07) than for the observed one (1.14 ± 0.05). We consider only the period 1900-2000 to construct the FM plot for the observed seismicity, as the Leydecker catalog is not complete for magnitude 5 before 1900. From the difference in the intercepts it is possible to estimate that a dimensionless unit of time corresponds to about 1500 years, thus our experiments cover a time interval of about 30,000 years.

The difference in the *b*-values obtained for observed and synthetic seismicity may be explained by the fact that the model does not reproduce with sufficient detail the fault network of the region under consideration. As shown by Keilis-Borok et al. (1997), when the movements of blocks have an essential rotation component (as in our case) the increase of the fragmentation of the block structure causes the decrease of the *b*-value for synthetic seismicity. Therefore, the insufficient representation of the fragmentation of the fault network in the model may cause the increase of the *b*-value for synthetic seismicity. The increase of the *b*-value for synthetic seismicity may be due also to the rough mechanism of earthquake occurrence used in the model that does not consider the 3D structure of the earthquake source and to other simplifications used in the model.

Accordingly to the analysis performed by Molchan et al. (1997) the *b*-value calculated for the observed seismicity in Northern and Central Italy is essentially larger than that in Southern Italy (excluding Sicily). The *b*-values calculated for these regions, either considering the synthetic seismicity and the earthquake catalog UCI2001; show a similar difference, in rather good agreement with the results of Molchan et al. (1997).

In the *North-Central Apennines* (faults 25, 26, 27, 28, and 29 in Fig. 3) the synthetic seismicity is represented by two belts. In agreement with the observations the western belt is more active than the eastern one. The largest synthetic events (with $M = 6.8$) occur nearby the junction between the Apennines and the Alps. Actually, some large events (e.g., the $M=6.7$ Garfagnana earthquake, occurred on September 1920), took place in the north-western part of the Apennines, corresponding to the location of fault 28, but the frequency observed for such events is not as high as that shown in Figure 4.

In the *Southern Apennines* (faults 30 and 32 in Fig. 3) the synthetic seismicity is represented by two belts, as well, and the level of the synthetic seismicity is higher than in North-Central Apennines, in agreement with the observations. The maximum synthetic magnitude equals 7.6. Here the largest observed earthquakes occurred in 1930 ($M = 7.5$) and 1857 ($M = 7.0$), and several events with $M \geq 6.5$ are reported.

In the *Calabrian arc* (faults 19 and 20 in Fig. 3) the level of the synthetic seismicity is high and the maximum synthetic magnitude is 7.3, not far from the value 7.1 of the largest observed earthquake (Messina, 1908).

At the *eastern edge of Adria* (faults 9 and 10 in Fig. 3), in the southern part of the Dinarides, the level of the synthetic seismicity, with a maximum synthetic magnitude 6.8, underestimates the observed seismicity, maximum magnitude 7.5. The highest synthetic seismicity is obtained in the Northern Dinarides, where several synthetic earthquakes with magnitude $M \geq 7.5$ occur, the largest having $M = 7.6$. The maximum magnitude observed here is the 7.9 earthquake occurred in 1348, in the vicinity of the conjunction of the Alps and the Dinarides.

At the *eastern edge of Sicily* (fault 15 in Fig. 3) the maximum synthetic magnitude is 7.2, while the largest observed earthquake with $M = 7.5$ occurred along the Malta escarpment in 1693; several events with $M \geq 6.5$ are reported.

In the *Southern Alps* (fault 24 in Fig. 3) the maximum synthetic magnitude is 6.6, and the largest observed earthquake, $M = 6.8$, occurred in 1222.

5.3 Source mechanisms

The source mechanisms of the synthetic earthquakes have been analyzed in different parts of the block model. The mechanism of an earthquake is routinely described by means of three angles: strike, dip, and slip (or rake). Strike and dip define the azimuth and the dip angle of the rupture plane, while the slip defines the direction of the displacement along the rupture plane. In the block model, strike and dip are prescribed by the geometry of the block structure; therefore the only free parameter is the slip. The values of slip have the following meaning: 90° and -90° correspond, respectively, to pure reverse and normal faulting, 0° and 180° indicate, respectively, right-lateral or left-lateral pure strike-slip mechanism, any other mechanism is described by slip values within the above limits.

The available source mechanisms of the observed earthquakes (e.g. Saraò et al., 1997, Vannucci et al., 2004), shown in Figure 5, are compared with the synthetic ones. We consider several sub-regions corresponding to different parts of the block structure and the observed fault plane solutions are divided into three groups: strike-slip (rake between -30° and 30° , or -150° and 150°), normal faulting (rake between -30° and -150°), and reverse faulting (rake between 30° and 150°). As a whole, the comparison of the mechanisms obtained in the model with the observations and the stress map of Italy (Montone et al., 1999) shows a good agreement.

For the North-Central Apennines (faults 28, 29 in Fig. 3) and the Southern Apennines (faults 30, 32 in Fig. 3) the histograms of the slip values obtained for the synthetic earthquakes are given in Figures 15 and 16. In both histograms the slip varies from -70° to -110° , with a peak nearby -90° , hence most of the synthetic earthquakes correspond to normal faulting. The dominating type of observed mechanisms is normal faulting, as can be seen from the percentage of the different observed fault plane solutions, shown in the same figures.

Similar histograms for the western margin of the Adria plate, along the North-Central Apennines (faults 25 and 26 in Fig. 3), are given in Figure 17. Here the histogram reaches its maximum nearby 120° that corresponds to reverse faulting, but normal faulting and strike-slip characterize part of the synthetic earthquakes. The observed fault plane solutions have a similar distribution.

The maximum in the histogram for the Southern Alps (fault 24 in Fig. 3) is between 105° and 85° (Fig. 18) that corresponds to reverse faulting, and it complies with the observations.

Most of the synthetic earthquakes obtained for the Calabrian Arc (faults 19 and 20 in Fig. 3) show normal faulting, like the observations, and the maximum in the histogram of the slip values is between -80° and -120° (Fig. 19).

The slip values of the synthetic earthquakes obtained for the eastern edge of Sicily (fault 15 in Fig. 3) are concentrated nearby -90° (Fig. 20). Hence, most of the synthetic earthquakes correspond to normal faulting, in fairly good agreement with the distribution of the observed fault plane solutions.

For the eastern edge of the Adria along the Dinarides (fault 9 in Fig. 3) the histogram of the slip values obtained for the synthetic earthquakes peaks between 70° and 50° that corresponds to reverse faulting with a considerable strike-slip component. For the south-eastern edge of the Adria (fault 10 in Fig. 3) the slip component increases, and the maximum of the slip histogram is between 30° and 10° (Fig. 21). The observations exhibit a similar behavior.

6. Conclusions

The results of the numerical simulation of block structure dynamics for the Italian region show that it is possible to reproduce the main observed features of the tectonic motions. The movements obtained as a result of the numerical simulation exhibit a good agreement with the available observations (GPS and VLBI). The extension belt along the Apennines and the contraction belt along the north-western boundary of the Adriatic Sea are correctly reproduced.

Figure 22 shows the distribution of the epicenters of observed and synthetic earthquakes with $M \geq 6.0$. The best consistency is reached in the belt passing through Sicily, Calabria, southern and central Apennines. The largest synthetic events are in the Malta escarpment, in the Calabrian arc, and in the Southern Apennines (to the south of the Ortona-Roccamonfina line); the rate of the synthetic seismic activity in the Apennines decreases from South to North. Nevertheless the level of the synthetic seismicity in the Northern Apennines and its conjunction with the Western Alps is too high in comparison with the observations, while there is a lack of large synthetic events in the Dinarides, especially in their southern part.

Few large synthetic earthquakes occur near the conjunction of the Dinarides and the Eastern Alps compared to observations. Synthetic seismicity in the Eastern Alps agrees with the observations, while it poorly correlates with observations in the Western Alps. A number of large earthquakes are observed there, while there are no large synthetic events.

The partial disagreement between observed and synthetic seismicity can be possibly explained by some of the features of the block structure geometry. The basis of our block structure is the seismotectonic scheme of Scandone et al. (1994). The separation of the Adria from the Apennines and the Eastern Alps can be easily inferred here, while the boundary between the Po valley and the Western Alps cannot be traced unambiguously. Correspondingly, the agreement between synthetic and observed seismicity is good in the Apennines and the Eastern Alps and it is poor in the Western Alps. The disagreement between observed and synthetic seismicity in the Dinarides may be caused also by incorrect reproduction of the relative movement of block VI and the boundary blocks BB2 and BB3. A revision of the block structure geometry using as additional information, for example, the morphostructural zoning of the study area (Gorshkov et al. 2002, Gorshkov et al. 2004), and specifying the relevant movements for the boundary blocks BB2 and BB3 may improve the results of the modeling and will be the subject of a forthcoming study.

The comparison of the distribution of the epicenters of synthetic earthquakes with $M \geq 6.0$ with the earthquake-prone areas, determined by Gorshkov et al. (2004) for the same magnitude cut-off (Fig. 23), shows that there is a rather good agreement in the Apennines, in the Malta escarpment, in the Calabrian arc and in the Eastern Alps. The agreement is poor in the Dinarides and there are no synthetic epicenters in the Western Alps but several earthquake-prone areas are identified there. The level of the synthetic seismicity is high and the earthquake-prone areas are numerous at the conjunction of the Northern Apennines with the Western Alps, though no earthquakes with $M \geq 6.0$ have been observed there (see Fig. 22). The correspondence between the results of the modeling of the block structure dynamics and of the identification of earthquake-prone areas, by the morphostructural zonation, could be an indication for a high seismic potential in this part (conjunction of the Northern Apennines with the Western Alps) of the study region.

The source mechanisms of the synthetic earthquakes are in a quite good agreement with the available observations (Saraò et al., 1997, Vannucci et al., 2004). Normal faulting is typical for the synthetic seismicity in the Apennines, the eastern edge of Sicily and the Calabrian arc, while reverse faulting predominates in the north-western boundary of the Adriatic Sea, in the Southern Alps and along the eastern edge of the Adria along the Dinarides.

The results of the modeling allow us to check some hypotheses about the tectonic processes controlling the geodynamics and seismicity in the study area. The main conclusion is that the available observations cannot be explained only as a consequence of the convergence of Africa and Europe, thus corroborating, with a very different modeling method, the results of previous studies. In particular, Bassi and Sabadini (1994) and Bassi et al. (1997) showed, by means of a thin-sheet viscous model, that subduction of the Ionian lithosphere underneath the Calabrian arc is necessary to explain the extensional style of the Tyrrhenian sea, and Jimenez-Munt et al. (2003), who used the thin-shell finite element approach to simulate active deformation in Mediterranean region, evidenced that the deformational style in the Mediterranean region is controlled by the Africa-Eurasia convergence and by the subduction in the Calabrian Arc and Aegean Sea.

The processes controlling the tectonics and the seismicity in the study region seem to be therefore quite complex. Introducing the rotation of the Adria plate around a rotation pole in the Western Alps, we obtain a relatively more credible movement of the block structure, and thus we indirectly support the hypothesis that the Adria is an independent, possibly fragmented (Oldow et al., 2002) microplate, compatibly with recent tomographic studies (Venisti et al., 2004). Battaglia et al., (2004) reached similar conclusion using GPS measurements and block modeling to study present-day deformations of the Adriatic region. At the same time there are some additional processes, connected with the passive subduction of the Ionian-Adria plate, which cause the coexistence of contraction and extension belts in the North-Central Apennines (Frepoli and Amato, 1997) and the high level of seismicity in the Calabrian Arc. The influence of the geometries and level of detail of the model as well as of the structural properties of the studied region, as reflected by the different coupling of the blocks with the underlying medium and by the differences in the rheology of fault zones, will be subject of forthcoming investigations.

Acknowledgements

These studies were partly done at the Abdus Salam International Center for Theoretical Physics, (Trieste, Italy) within the framework of the SAND group activity and supported by the International Science and Technology Center (project #1538), by NATO (SFP project 972266), by Grant #1269-2003-05 of the President of the Russian Federation for supporting leading scientific schools, and by James S. McDonnell Foundation within the framework of the 21st Century Collaborative Activity Award for Studying Complex Systems (project “*Understanding*

and Prediction of Critical Transitions in Complex Systems”). This is a contribution to the MIUR-COFINANZIAMENTO (projects 2001 and 2002).

References

- Aifa, T., Feinberg, H., and Pozzi, J. P. (1988), *Pliocene-Pleistocene evolution of the Tyrrhenian arc: paleomagnetic determination of uplift and rotational deformation*, Earth and Planet. Sci. Lett. 87, 438-452.
- Anderson, H., and Jackson, J. (1987), *Active tectonics in the Adriatic region*, Geophys. J. R. Astr. Soc. 91, 937-983.
- Anzidei, M., Baldi, P., Casula, G., Crespi, M., and Riguzzi, F. (1996), *Repeated GPS surveys across the Ionian Sea: evidence of crustal deformations*, Geophys. J. Int. 127, 257-267.
- Bassi, G., and Sabadini, R. (1994), *The importance of subduction for the modern stress field in the Tyrrhenian area*. Geophys. Res. Lett. 21, 329-332.
- Bassi, G., Sabadini, R., and Rebaï, S. (1997), *Modern Tectonic regime in the Tyrrhenian area: observations and models*, Geophys. J. Int. 129, 330-346.
- Battaglia, M., Murray, M., Serpelloni, E., and Bürgmann, R. (2004), *The Adriatic region: An independent microplate within the Africa-Eurasia collision zone*, Geophys. Res. Lett. 31, L09605, doi:10.1029/2004GL019723.
- Benedetti, L. (1999), *Sismotectonique de l'Italie et des Régions Adjacentes: Fragmentation du Promontoire Adriatique*, Ph.D. thesis, Université Paris VII, pp. 354.
- Brockmann, E., Calais, E., Douša, J., Gendt, G., Ge, M., Higgins, M., Johansson, J., van der Maarel, H., Offiler, D., Rius, A., and Vespe, F. (2001), *The COST-716 benchmark GPS campaign for numerical weather prediction applications*, Geophysical Research Abstracts 3. Abstracts of the Contributions of the 26th General Assembly of the European Geophysical Society, A-02674.
- Buck, R. (2003). *Consequences of asthenospheric variability on continental rifting*. In *Reology and Deformation of the Lithosphere at Continental Margins* (eds. Karner, G. D. et al.) (Columbia University Press, New York) pp. 1-30.
- Burridge, R., and Knopoff, L. (1967), *Model and theoretical seismicity*, Bull. Seismol. Soc. Am. 57, 341-360.
- Calais, E., Galisson, L., Stéphan, J.-F., Delteil, J., Deverchère, J., Larroque, C., Mercier de Lépinay, B., Popoff, M., and Sosson, M. (2000), *Crustal strain in the Southern Alps, France, 1948-1998*, Tectonophysics 319, 1-17.
- Calcagnile, G., and Panza, G. F. (1981), *The main characteristics of the lithosphere-asthenosphere system in Italy and surrounding regions*, Pure Appl. Geophys. 119, 865-879.
- Caputo, M., Panza, G. F., and Postpischl, D. (1970), *Deep structure of the Mediterranean basin*, JGREA 75, 4919.
- Caputo, M., Panza, G. F., and Postpischl, D. (1972), *New evidence about the deep structure of the Lipari arc*, Tectonophysics 15, 219.
- Chimera, G., Aoudia, A., Saraò, A., and Panza, G. F. (2003), *Active tectonics in Central Italy: constraints from surface wave tomography and source moment tensor inversion*, Phys. Earth Planet. Inter. 138, 241-262.
- Cianetti, S., Gasperini, P., Bokaletti, M., and Ciunchi, C. (1997), *Reproducing the velocity and stress Fields in the Aegean region*, Geophys. Res. Lett. 24, 2087-2090.
- Cisternas, A., Godefroy, P., Gvishiani, A., Gorshkov, A. I., Kosobokov, V., Lambert, M., Ranzman, E., Sallantin, J., Saldano, H., Soloviev, A., and Weber, C. (1985), *A dual approach to recognition of earthquake prone areas in the western Alps*, Annales Geophysicae 3, 249-270.

- Della Vedova, B., Marson, I., Panza, G. F., and Suhadolc, P. (1991), *Upper mantle properties of the Tuscan-Tyrrhenian area: a key for understanding the recent tectonic evolution of the Italian region*, *Tectonophysics* 195, 311-318.
- Della Vedova, B., Bellani, S., Pellis, G., and Squarci, P. (2001), *Deep temperatures and surface heat flow distribution*. In *Anatomy of an Orogen: the Apennines and Adjacent Mediterranean Basins* (eds. Vai, G. B., and Martini, I. P.) (Kluwer Academic Publisher) pp. 65-76.
- DeMets, C., Gordon, R. G., Argus, D. F., and Stein, S. (1990), *Current plate motions*, *Geophys. J. Int.* 101, 425-478.
- DeMets, C., Gordon, R. G., Argus, D. F., and Stein, S. (1994), *Effect of recent revisions to the geomagnetic reversal time scale on estimates of current plate motions*, *Geophys. Res. Lett.* 21, 2191-2194.
- Devoti, R., et al. (2002), *Geophysical interpretation of geodetic deformations in the Central Mediterranean area*. In *Plate Boundary Zones* (eds. Stein, S., and Freymueller, J. T.), *Geodynam. Ser.*, vol. 30, pp. 57-65.
- Dogliani, C. (1991), *A proposal of kinematic modeling for W-dipping subductions - Possible applications to the Tyrrhenian-Apennines system*, *Terra Nova* 3, 423-434
- Dogliani, C., Gueguen, E., Harabaglia, P., and Mongelli, F. (1999a), *On the origin of west-directed subduction zones and application to the western Mediterranean*. In *The Mediterranean Basins: Tertiary Extension within the Alpine Orogen* (eds. Durand, B. et al.) (Geological Society, London) Special Publications, vol. 156, pp. 541-561.
- Dogliani, C., Harabaglia, P., Merlini, S., Mongelli, F., Pecerrillo, A., and Piromallo, C. (1999b), *Orogens and slabs vs. their direction of subduction*, *Earth-Science Reviews* 45, 167-208.
- Frepoli, A., and Amato, A. (1997), *Contemporaneous extension and compression in the Northern Apennines from earthquake fault-plane solutions*, *Geophys. J. Int.* 129, 368-388.
- Gabrielov, A. M., Levshina, T. A., and Rotwain, I. M. (1990), *Block model of earthquake sequence*, *Phys. Earth Planet. Inter.* 61, 18-28.
- Geiger, A., Kahle, H-G., and Gubler, E. (1986), *Recent crustal movements in the Alpine-Mediterranean region analyzed in the Swiss Alps*, *Tectonophysics* 130, 289-298.
- Giunchi, C., Kiratzi, A., Sabadini, R., and Louvari, E. (1996), *A numerical model of the Hellenic subduction zone: Active stress field and sea-level changes*, *Geophys. Res. Lett.* 23, 2485-2488.
- Gorshkov, A. I., Panza, G. F., Soloviev, A. A., and Aoudia, A. (2002), *Morphostructural zonation and preliminary recognition of seismogenic nodes around the Adria margin in peninsular Italy and Sicily*, *Journal of Seismology and Earthquake Engineering* 3, 1-24.
- Gorshkov, A. I., Panza, G. F., Soloviev, A. A., and Aoudia, A. (2004), *Identification of seismogenic nodes in the Alps and Dinarides*, *Bool. Soc. Geol. It.* 123, 3-18.
- Gripp, A. E., and Gordon, R. G. (1990), *Current plate velocities relative to the hotspots incorporating the NUVEL-1 global plate motion model*, *Geophys. Res. Lett.* 17, 1109-1112.
- Gubler, E., Kahle, H-G., and Klingele, E. (1981), *Recent crustal movements in Switzerland and their geophysical interpretation*, *Tectonophysics* 71, 125-152.
- Ismail-Zadeh, A. T., Keilis-Borok, V. I., and Soloviev, A. A. (1999), *Numerical modeling of earthquake flow in the south-eastern Carpathians (Vrancea): effect of a sinking slab*, *Phys. Earth Planet. Inter.* 111, 267-274.
- Jackson J. (2003), *Velocity fields, faulting and strength on the continents*. In *Reology and Deformation of the Lithosphere at Continental Margins* (eds. Karner, G. D. et al.) (Columbia University Press, New York) pp. 31-45.
- Jimenez-Munt, I., Sabadini, R., and Gardi, A. (2003), *Active deformation in the Mediterranean from Gibraltar to Anatolia inferred from numerical modeling and geodetic and seismological data*, *J. Geophys. Res.* 108 (B1), 1-24.

- Karner, G. D., Taylor, B., Driscoll, N. W., and Kohlstedt, D. L. (Eds.) (2003), *Rheology and Deformation of the Lithosphere at Continental Margins* (Columbia University Press, New York).
- Keilis-Borok, V. I., Rotwain, I. M., and Soloviev, A. A. (1997), *Numerical modelling of block structure dynamics: dependence of a synthetic earthquake flow on the structure separateness and boundary movements*, *J. Seismol.* 1, 151-160.
- Keilis-Borok, V. I., and Soloviev, A. A. (Eds.) (2003), *Nonlinear Dynamics of the Lithosphere and Earthquake Prediction* (Springer-Verlag, Berlin-Heidelberg).
- Leydecker, G. (1991), *Historical Earthquake Catalogues: Central and southeastern Europe (342 BC - 1990)*, <http://www.bgr.de/quakecat/eng/homepage.htm>.
- Lundgren, P., Giardini, D., and Russo, R. M. (1998), *A geodynamic framework for eastern Mediterranean kinematics*, *Geophys. Res. Lett.* 25, 4007-4010.
- Maksimov, V. I., and Soloviev, A. A. (1999), *Clustering of earthquakes in a block model of lithosphere dynamics*. In *Computational Seismology and Geodynamics* (ed. Chowdhury, D. K.), vol. 4 (Am. Geophys. Union, Washington, D.C.) pp. 124-126.
- Marson, I., Panza, G. F., and Suhadolc, P. (1995), *Crust and upper mantle models along the active Tyrrhenian rim*. *Terra Nova* 7, 348-357.
- Meijer, R. T., and Wortel, J. R. (1996), *Temporal variation in the stress field of the Aegean region*, *Geophys. Res. Lett.* 23, 439-442.
- Meletti, C., Patacca, E., and Scandone, P. (1995), *Il sistema compressione-distensione in Appennino*. In *Cinquanta anni di attività didattica e scientifica del Prof. Felice Ippolito* (eds. Bonardi, G. et al.) (Liguori, Napoli) pp. 361-370.
- Meletti, C., Patacca, E., and Scandone, P. (2000), *Construction of a seismotectonic model: the case of Italy*, *Pure Appl. Geophys.* 157, 11-35.
- Molchan, G., Kronrod, T., and Panza, G. F. (1997), *Multi-scale seismicity model for seismic risk*, *Bull. Seismol. Soc. Am.* 87, 1220-1229.
- Montone, P., Amato, A., and Pondrelli, S. (1999), *Active stress map of Italy*, *J. Geophys. Res.* 104, 25595-25610.
- Mueller, B., Reinecker, J., Heidbach, O., and Fuchs, K. (2000), *The 2000 release of the World Stress Map*, <http://www.world-stress-map.org>.
- Murray, M., and Segall, P. (2001), *Modeling broadscale deformation in northern California and Nevada from plate motions and elastic strain accumulation*, *Geophys. Res. Lett.* 28, 4315-4318.
- Oldow, J. S., Ferranti, L., Lewis, D. S., Campbell, J. K., D'Argenio, B., Catalano, R., Pappone, G., Carmignani, L., Conti, P., and Aiken, C. L. V. (2002), *Active fragmentation of Adria, the north Africa promontory, central Mediterranean orogen*, *Geology* 30, 779-782.
- Negredo, A. M., Sabadini, R., Bianco, G., and Fernandez, M. (1999), *Three-dimensional modeling of crustal motions caused by subduction and continental convergence in the Central Mediterranean*, *Geophys. J. Int.* 136, 261-274.
- Nocquet, J. M., and Calais, E. (2003), *Crustal velocity field of western Europe from permanent GPS array solutions, 1996-2001*, *Geophys. J. Int.* 154, 72-88.
- Pamic, J., Balen, D., and Herak, M. (2002), *Origin and geodynamic evolution of Late Paleogene magmatic associations along the Periadriatic-Sava-Vardar magmatic belt*, *Geodinamica Acta* 15, 209-231.
- Panza, G. F. (1984), *Structure of the lithosphere-asthenosphere system in the Mediterranean region*, *Annales Geophys.* 2, 137-138.
- Panza, G. F., Mueller, S., Calcagnile, G., and Knopoff, L. (1982), *Delineation of the north central Italian upper mantle anomaly*, *Nature* 296, 238-239.
- Panza, G. F., Soloviev, A. A., and Vorobieva, I. A. (1997), *Numerical modeling of block-structure dynamics: Application to the Vrancea region*, *Pure Appl. Geophys.* 149, 313-336.

- Panza, G. F., Pontevivo, A., Chimera, G., Raykova, R., and Aoudia, A. (2003), *The Lithosphere-Asthenosphere: Italy and surroundings*, Episodes 26, 169-174.
- Pasquale, V., Verdoya, M., Chiozzi, P., and Ranalli G. (1997), *Rheology and seismotectonic regime in the northern central Mediterranean*, Tectonophysics 270, 239-257.
- Peresan, A. and Panza, G. F. (2002), *UCI2001: The Updated Catalogue of Italy*, ICTP, Trieste, Internal report, IC/IR/2002/3.
- Pollack, H., Hurter, J., and Johnson, R. (1993), *Heat loss from the Earth's interior: Analysis of the global data set*, Rev. Geophys, 31, 267-280.
- Press, F., and Allen, C. (1995), *Patterns of seismic release in the southern California region*, J. Geophys. Res. 100, 6421-6430.
- Sagnotti, L. (1992), *Paleomagnetic evidence for a Pleistocene counterclockwise rotation of the Sant'Arcangelo basin, Southern Italy*, Geophys. Res. Lett. 19, 135-138.
- Sagnotti, L., Facenna, C., and Funicello, R. (1994), *Paleomagnetic evidence for no tectonic rotation of the Central Italy Tyrrhenian margin since upper Pliocene*, Geophys. Res. Lett. 21, 481-484.
- Sarà, A., Panza, G. F., and Suhadolc, P. (1997), *Waveforms and polarities for extended and point source studies. Earthquake fault plane solutions: data bases, derived parameters, geodynamic inferences*. In *Proceedings of the Messina University Forum on "Geodynamics of the Calabrian Arc"* (Taormina, Messina, Italy) pp. 13-17.
- Scandone, P., Patacca, E., Meletti, C., Bellatalla, M., Perilli, N., and Santini, U. (1990), *Struttura geologica, evoluzione cinematica e schema sismotettonico della penisola italiana*, Atti del Convegno GNDT 1, 119-135.
- Scandone, P., Patacca, E., Meletti, C., Bellatalla, M., Perilli, N., and Santini, U. (1994), *Seismotectonic zoning of the Italian peninsula: revised version*, Working file NOV94.
- Schmid, S. M., Pfiffner, A., Froitzheim, N., Schonborn, G., and Kissling, E. (1996), *Geophysical-geological transect and tectonic evolution of the Swiss-Italian Alps*, Tectonics 15, 1036-1064.
- Soloviev, A. A., Vorobieva, I. A., and Panza, G. F. (1999), *Modelling of block-structure dynamics: Parametric study for Vrancea*, Pure Appl. Geophys. 156, 395-420.
- Soloviev, A. A., Vorobieva, I. A., and Panza, G. F. (2000), *Modelling of block structure dynamics for the Vrancea region: Source mechanisms of the synthetic earthquakes*, Pure Appl. Geophys. 157, 97-110.
- Soloviev, A., and Ismail-Zadeh, A. (2003), *Models of dynamics of block-and-fault systems*, In *Nonlinear Dynamics of the Lithosphere and Earthquake Prediction* (eds. Keilis-Borok, V. I., and Soloviev, A. A.) (Springer-Verlag, Berlin-Heidelberg) pp. 71-139.
- Sobolev, P. O., and Rundquist, D. V. (1998), *The relationship between seismicity and geodynamics in the Tethys collision belt*, Doklady Earth Sciences 361, 700-705.
- Utsu, T., and Seki, A. (1954), *A relation between the area of aftershock region and the energy of main shock*, J. Seismol. Soc. Japan 7, 233-240.
- Vannucci, G., Pondrelli, S., Argnani, A., Morelli, A., Gasperini, P., and Boschi, E. (2004), *An Atlas of Mediterranean Seismicity*, Annales Geophys., Suppl. 47 (1).
- Venisti, N., Calcagnile, G., Pontevivo, A., and Panza, G. F. (2004), *Tomographic study of the Adriatic plate*, Pure Appl. Geophys., in press.
- Vorobieva, I. A., Gorshkov, A. I., and Soloviev, A. A. (2000), *Modelling of the block structure dynamics and seismicity for the Western Alps*. In *Computational Seismology*, vol. 31 (GEOS, Moscow) pp. 154-169 (in Russian).
- Ward, S. N. (1994), *Constraints on the seismotectonics of the Central Mediterranean from Very Long Baseline Interferometry*, Geophys. J. Int. 117, 441-452.
- Yamashita, T., and Knopoff, L. (1992), *Model for intermediate-term precursory clustering of earthquakes*, J. Geophys. Res. 97, 19873-19879.

Table 1 - Experiment 1 (standard set)

Block	Prescribed velocities of underlying medium in cm per unit of dimensionless time		Resulting displacements and rotations of blocks		
	V _x	V _y	dX(cm)	dY(cm)	Angle (10 ⁻⁶ rad)
I	0	0	-26.01	-2.93	1.34
II	0	0	-3.97	6.68	-0.39
III	0	0	-22.71	2.56	2.02
IV	0	0	-66.59	91.84	5.17
V	0	0	24.33	11.60	-0.08
VI	0	0	102.90	261.46	16.09
VII	0	0	-68.06	55.15	-2.48
VIII	0	0	-151.22	197.53	-0.89
IX	0	0	-60.36	50.70	-6.55
X	0	0	-190.28	175.40	-19.35
XI	0	0	80.57	59.50	9.12

Prescribed velocities of boundary blocks in cm per unit of dimensionless time			
Boundary block	V _x	V _y	
BB1-BB3, BB6-BB9	0	0	
BB4	-25.00	65.00	
BB5	-25.00	65.00	

The prescribed angle velocity $\omega = 0$ for all boundary blocks and medium underlying blocks of structure in all experiments.

Table 2 - Experiment 2

Block	Prescribed velocities of underlying medium in cm per unit of dimensionless time		Resulting displacements and rotations of blocks		
	V _x	V _y	dX(cm)	dY(cm)	Angle (10 ⁻⁶ rad)
I	0	0	-6.86	-0.17	0.28
II	0	0	-2.32	2.07	-0.17
III	0	0	-6.63	-0.81	0.59
IV	0	0	-27.33	36.98	2.19
V	0	0	7.70	0.85	0.22
VI	0	0	32.57	114.34	7.58
VII	0	0	-31.55	40.09	-1.93
VIII	0	0	-87.08	103.98	-1.21
IX	0	0	-27.68	28.84	-5.30
X	0	0	-140.00	106.26	-16.18
XI	0	0	30.19	24.97	4.39

Prescribed velocities of boundary blocks in cm per unit of dimensionless time			
Boundary block	V _x	V _y	
BB1-BB3, BB6-BB9	0	0	
BB4	-25.00	65.00	
BB5	-25.00	65.00	

Table 3 - Experiment 3

Block	Prescribed velocities of underlying medium in cm per unit of dimensionless time		Resulting displacements and rotations of blocks		
	V _x	V _y	dX(cm)	dY(cm)	Angle (10 ⁻⁶ rad)
I	0	0	-148.48	108.06	12.90
II	0	0	37.31	96.13	-1.54
III	0	0	4.68	119.94	1.90
IV	1.20	45.60	33.94	767.95	8.49
V	33.30	54.60	406.57	823.74	26.11
VI	33.50	77.30	673.85	1340.63	8.07
VII	062.70	65.000	783.82	317.88	-21.06
VIII	69.60	74.10	1286.22	1373.10	-0.94
IX	0	0	73.57	132.34	0.57
X	0	0	-355.93	1191.13	1.02
XI	44.40	63.70	720.75	1125.58	19.83

Prescribed velocities of boundary blocks in cm per unit of dimensionless time				
Boundary block	V _x	V _y		
BB1-BB3, BB6-BB9	0	0		
BB4	69.60	74.10		
BB5	-25.00	65.00		

Table 4 - Experiment 4

Block	Prescribed velocities of underlying medium in cm per unit of dimensionless time		Resulting displacements and rotations of blocks		
	V _x	V _y	dX(cm)	dY(cm)	Angle (10 ⁻⁶ rad)
I	0	0	-139.14	110.16	12.46
II	0	0	39.52	99.14	-1.58
III	55.00	45.00	461.27	652.64	-6.06
IV	1.20	45.60	107.54	834.56	7.10
V	33.30	54.60	491.55	837.78	19.54
VI	33.50	77.30	677.09	1342.99	7.09
VII	062.70	65.000	766.86	325.59	-22.89
VIII	69.60	74.10	1284.96	1373.72	-0.98
IX	0	0	-256.30	189.63	9.63
X	0	0	-365.48	1198.77	1.49
XI	44.40	63.70	741.79	1096.82	22.15

Prescribed velocities of boundary blocks in cm per unit of dimensionless time				
Boundary block	V _x	V _y		
BB1-BB3, BB6, BB8-BB9	0	0		
BB4	69.60	74.10		
BB5	-25.00	65.00		
BB7	-30.00	30.00		

Table 5 - Experiment 5

Block	Prescribed velocities of underlying medium in cm per unit of dimensionless time		Resulting displacements and rotations of blocks		
	V _x	V _y	dX(cm)	dY(cm)	Angle (10 ⁻⁶ rad)
I	0	0	-129.80	100.92	11.58
II	0	0	33.70	89.27	-1.22
III	55.00	45.00	638.37	728.83	-11.13
IV	1.20	45.60	123.90	842.10	7.25
V	33.30	54.60	549.00	867.17	17.45
VI	33.50	77.30	680.59	1341.60	7.19
VII	062.70	65.000	920.18	399.97	-17.08
VIII	69.60	74.10	1295.89	1371.29	-0.86
IX	0	0	-255.99	189.50	9.66
X	0	0	-365.82	1199.15	1.49
XI	44.40	63.70	757.07	1095.01	21.82

Prescribed velocities of boundary blocks in cm per unit of dimensionless time			
Boundary block	V _x	V _y	
BB1-BB3, BB6, BB8-BB9	0	0	
BB4	69.60	74.10	
BB5	-25.00	65.00	
BB7	-30.00	30.00	

Table 6 - Experiment 6

Block	Prescribed velocities of underlying medium in cm per unit of dimensionless time		Resulting displacements and rotations of blocks		
	V _x	V _y	dX(cm)	dY(cm)	Angle (10 ⁻⁶ rad)
I	0	0	-141.84	110.46	11.85
II	0	0	13.07	125.18	-0.56
III	55.00	45.00	929.60	904.87	-15.68
IV	1.20	45.60	133.55	878.23	6.54
V	33.30	54.60	708.52	1031.95	8.34
VI	33.50	77.30	723.40	1395.68	6.11
VII	062.70	65.000	1216.02	493.51	-1.59
VIII	69.60	74.10	1373.14	1416.92	-0.06
IX	0	0	1.10	62.15	1.25
X	0	0	-436.41	1266.30	0.53
XI	44.40	63.70	822.69	1171.53	20.44

Prescribed velocities of boundary blocks in cm per unit of dimensionless time			
Boundary block	V _x	V _y	
BB1-BB3, BB6, BB8-BB9	0	0	
BB4	69.60	74.10	
BB5	-25.00	65.00	
BB7	-30.00	30.00	

Figure captions

Fig. 1 - Definitions used in the block-structure model.

Fig. 2 - Geodynamic model of Italy: structural sketch from Meletti et al. (2000).

Fig. 3 - Geometry of the block structure. I – XI – blocks; BB1- BB9 – boundary blocks.

Fig. 4 - Observed seismicity with $M \geq 5.5$, 1000-2000, (Peresan and Panza. 2002, Leydecker. 1991) and geometry of the block structure.

Fig. 5 - Observed fault plane solutions in the modeled region (Saraò et al., 1997).

Fig. 6 - Scheme describing the modeling of non-horizontal movements (e.g. uprising mantle flow or gravity) in the two-dimensional model of the block structure dynamics.

Fig. 7 - Synthetic seismicity and movements of block structure: Experiment 1

Fig. 8 - Synthetic seismicity and movements of block structure: Experiment 2.

Fig. 9 - Synthetic seismicity and movements of block structure: Experiment 3.

Fig. 10 - Synthetic seismicity and movements of block structure: Experiment 4.

Fig. 11 - Synthetic seismicity and movements of block structure: Experiment 5.

Fig. 12 - Synthetic seismicity and geometry of block structure: Experiment 6.

Fig. 13 – Comparison of the movements (open arrows) obtained in the numerical simulation of experiment 6 with the observations (fill arrows) (Devoti et al. 2002). The size of symbols is proportional to the values given in Table 6.

Fig. 14 - Frequency-magnitude distribution for the synthetic (full circles) and observed (open circles) seismicity.

Fig. 15 - Distribution of the slip angles for the synthetic and observed earthquakes along the North-Central Apennines (faults 28, 29 in Fig. 3).

Fig. 16 - Distribution of the slip angles for the synthetic and observed earthquakes (Saraò et al., 1997). along the Southern Apennines (faults 30, 32 in Fig. 3).

Fig. 17 - Distribution of the slip angles for the synthetic and observed earthquakes (Saraò et al., 1997) along the contraction belt in North-Central Apennines (faults 25, 26 and 27 in Fig. 3).

Fig. 18 - Distribution of the slip angles for the synthetic and observed earthquakes (Saraò et al., 1997) in the Southern Alps (fault 24 in Fig. 3).

Fig. 19 - Distribution of the slip angles for the synthetic and observed (Saraò et al., 1997) earthquakes in the Calabrian Arc (faults 19 and 20 in Fig. 3).

Fig. 20 - Distribution of the slip angles for the synthetic and observed (Saraò et al., 1997) earthquakes at the eastern edge of Sicily (fault 15 in Fig. 3).

Fig. 21 - Distribution of the slip angles for the synthetic and observed earthquakes (Saraò et al., 1997) at the eastern edge of Adria (faults 9 and 10 in Fig. 3).

Fig. 22 – Comparison of the synthetic (Experiment 6) and observed 1000-2000, (Peresan and Panza. 2002, Leydecker. 1991) seismicity with magnitude $M \geq 6.0$.

Fig. 23 - Synthetic earthquakes with $M \geq 6$ (Experiment 6) and seismogenic nodes (Gorshkov et al., 2002).

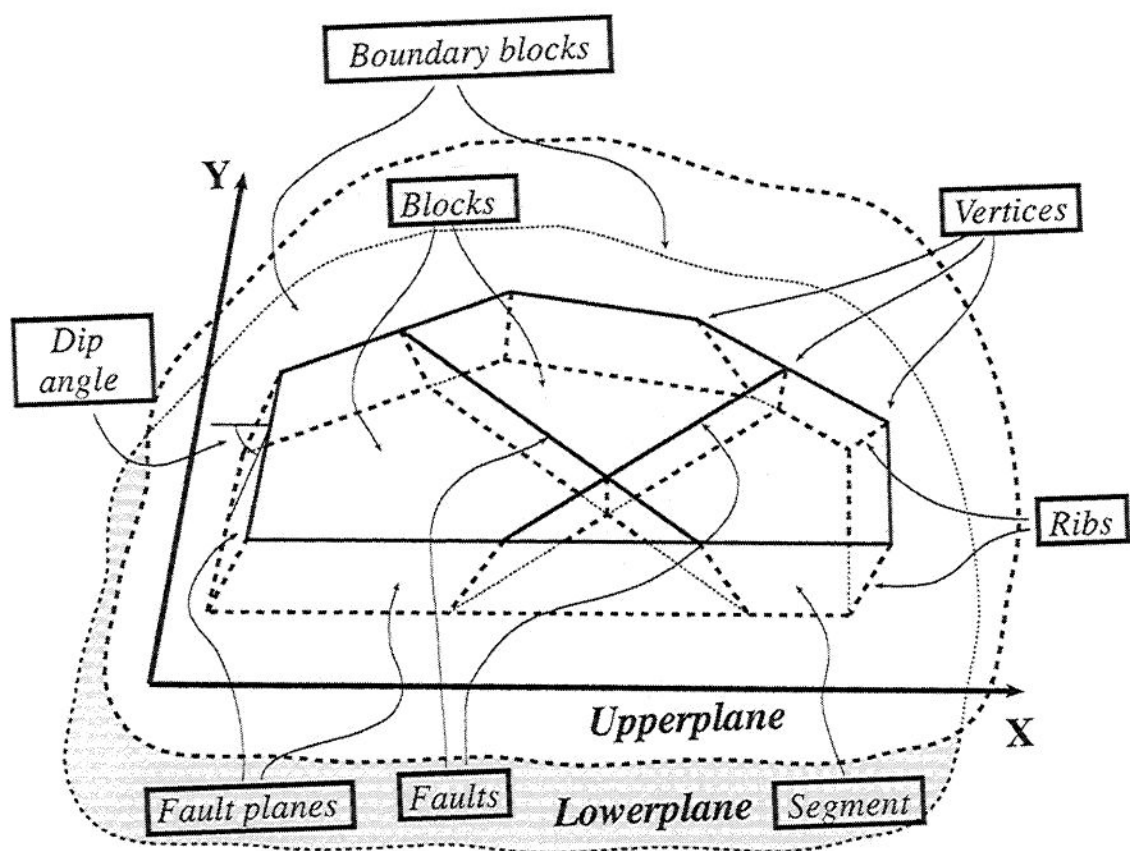


Figure 1

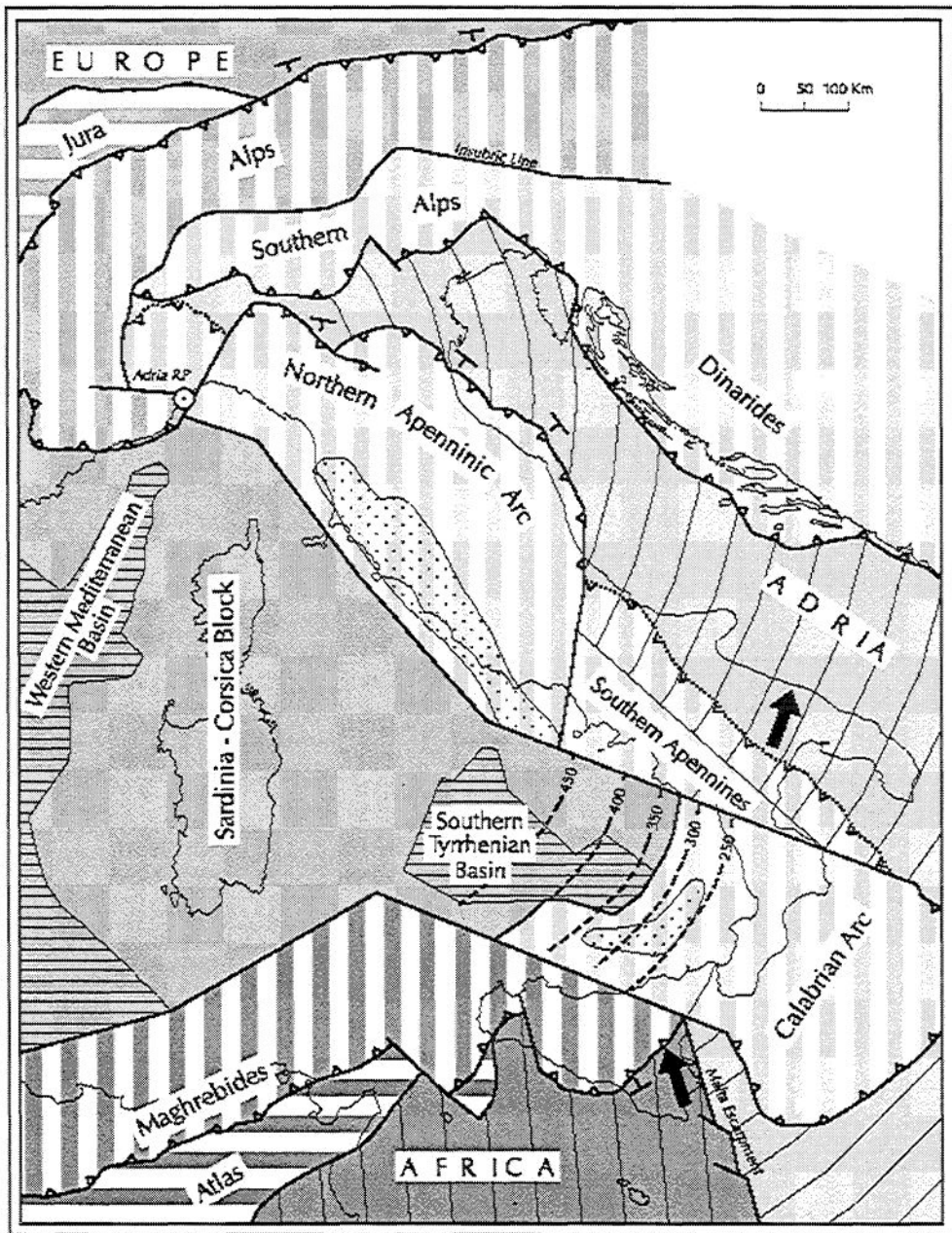


Figure 2

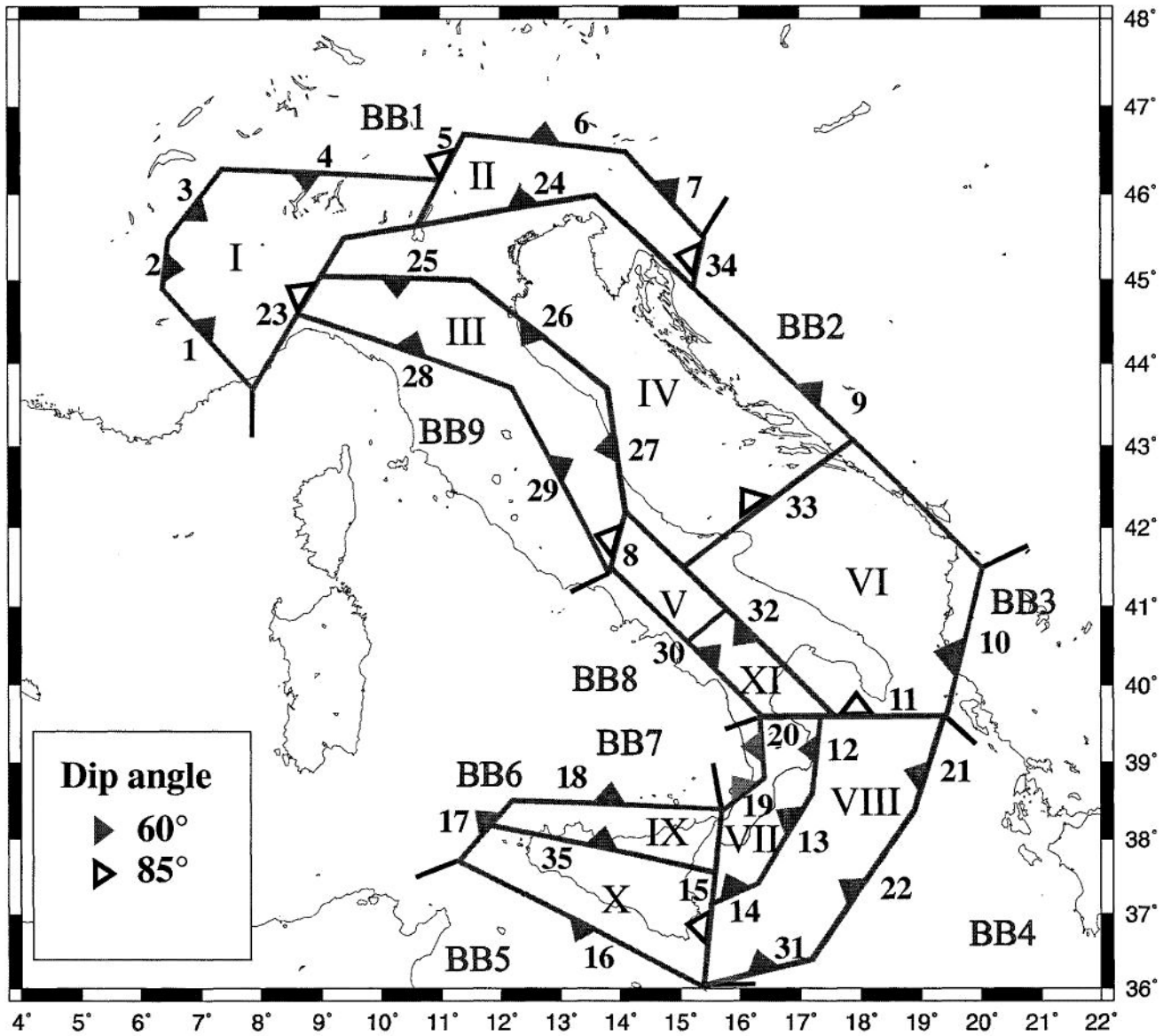


Figure 3

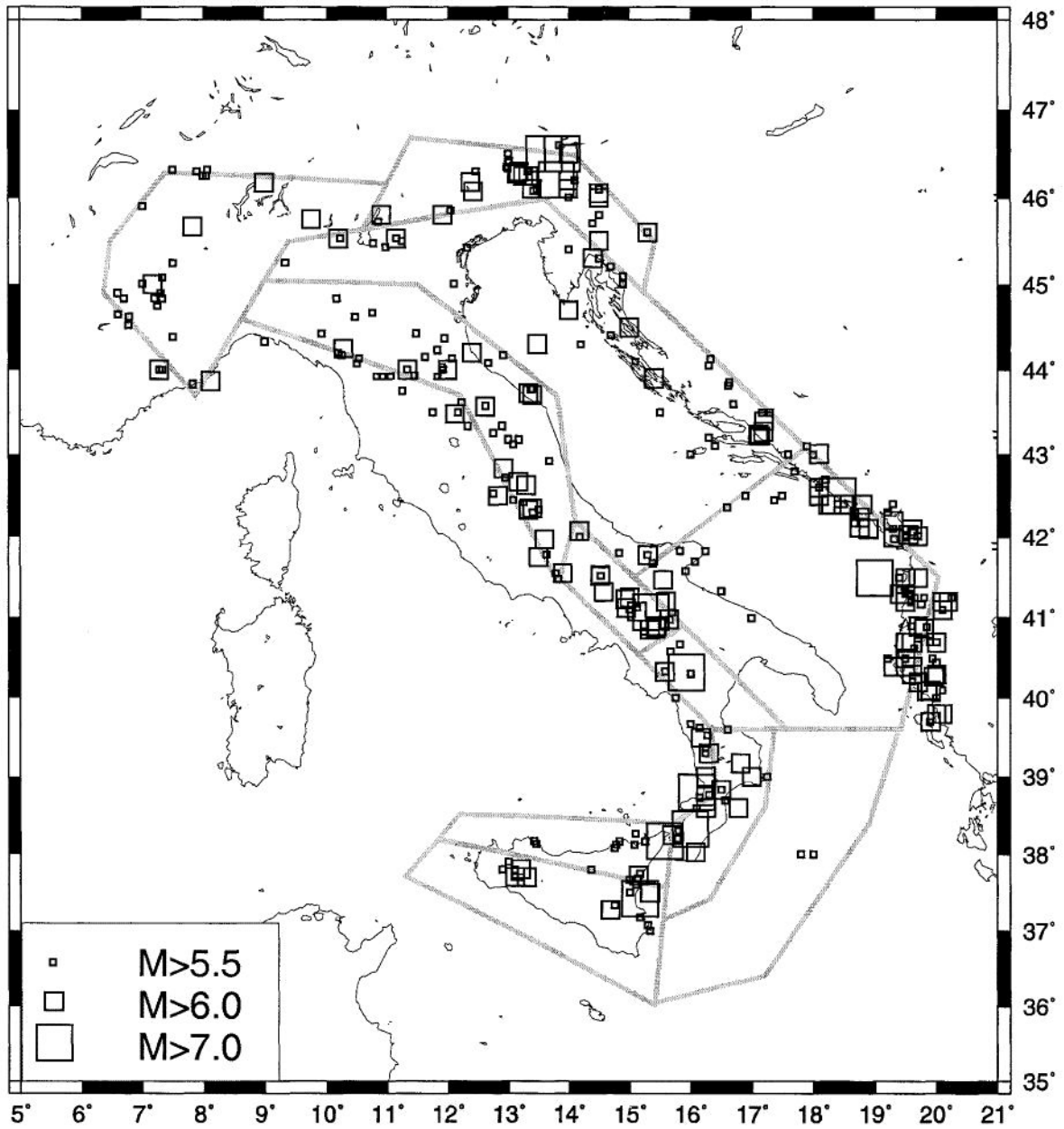


Figure 4

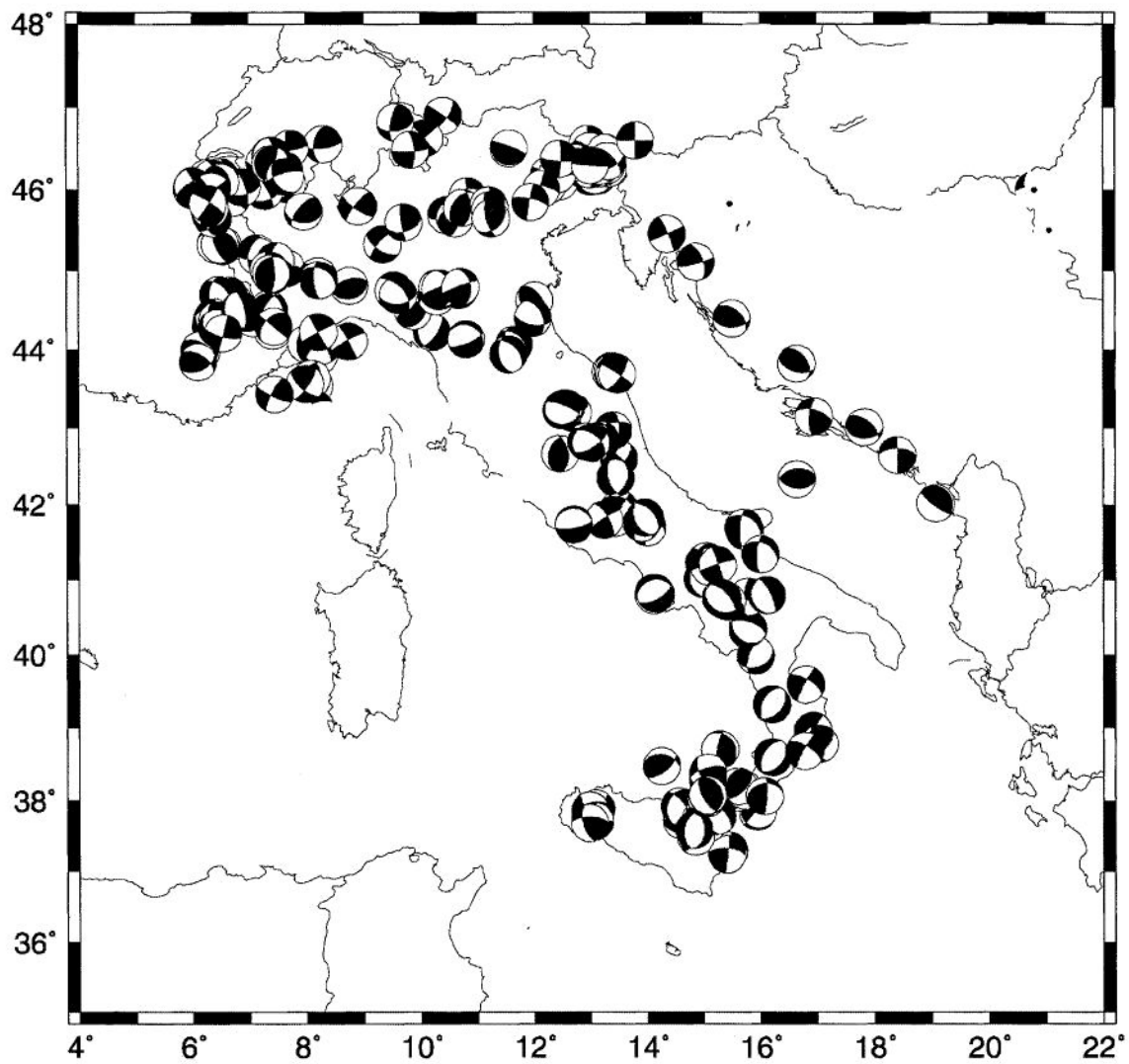
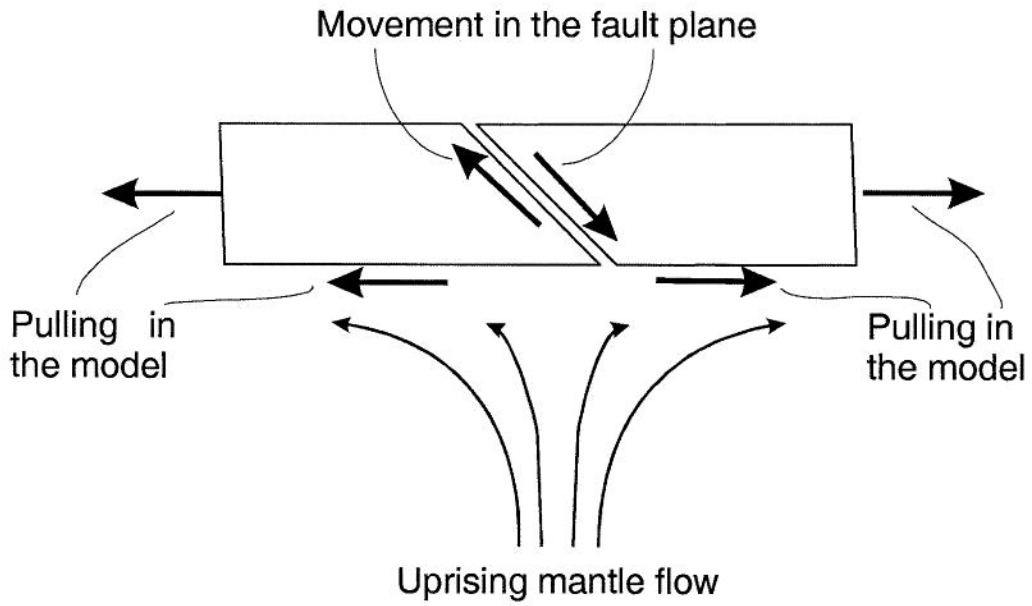


Figure 5

Extension



Contraction

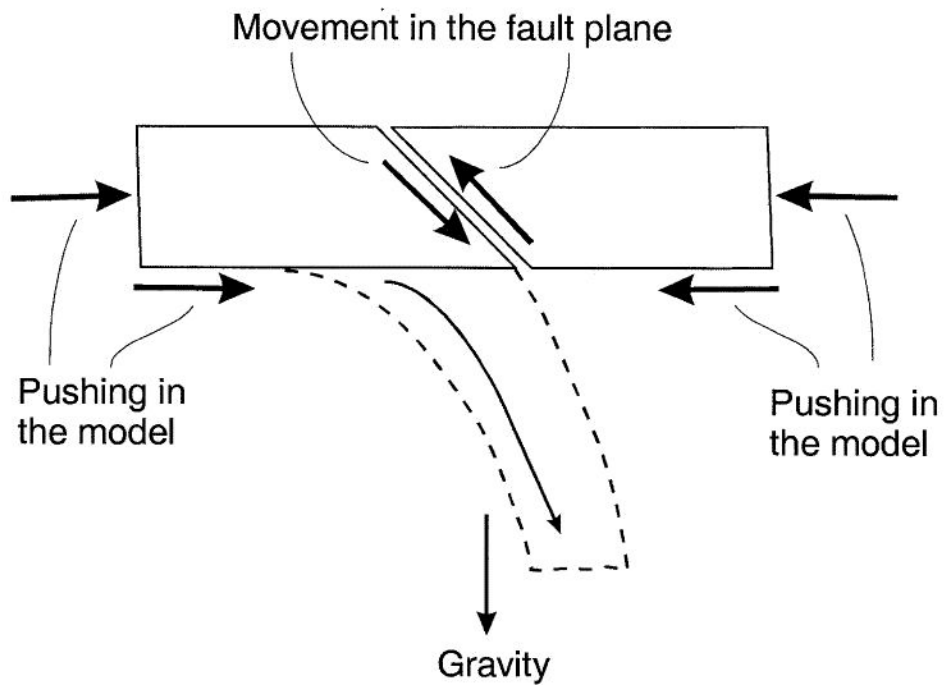
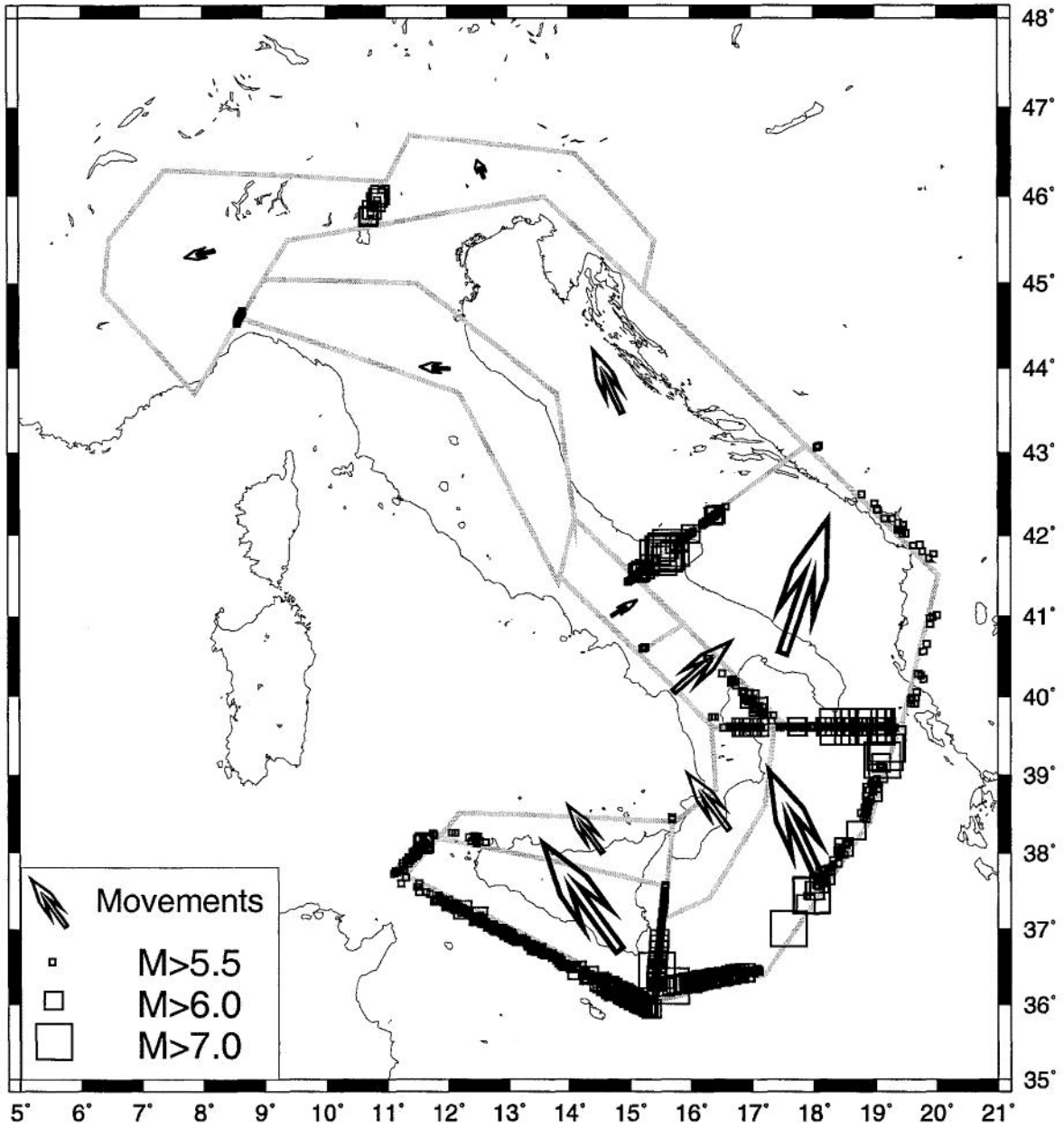
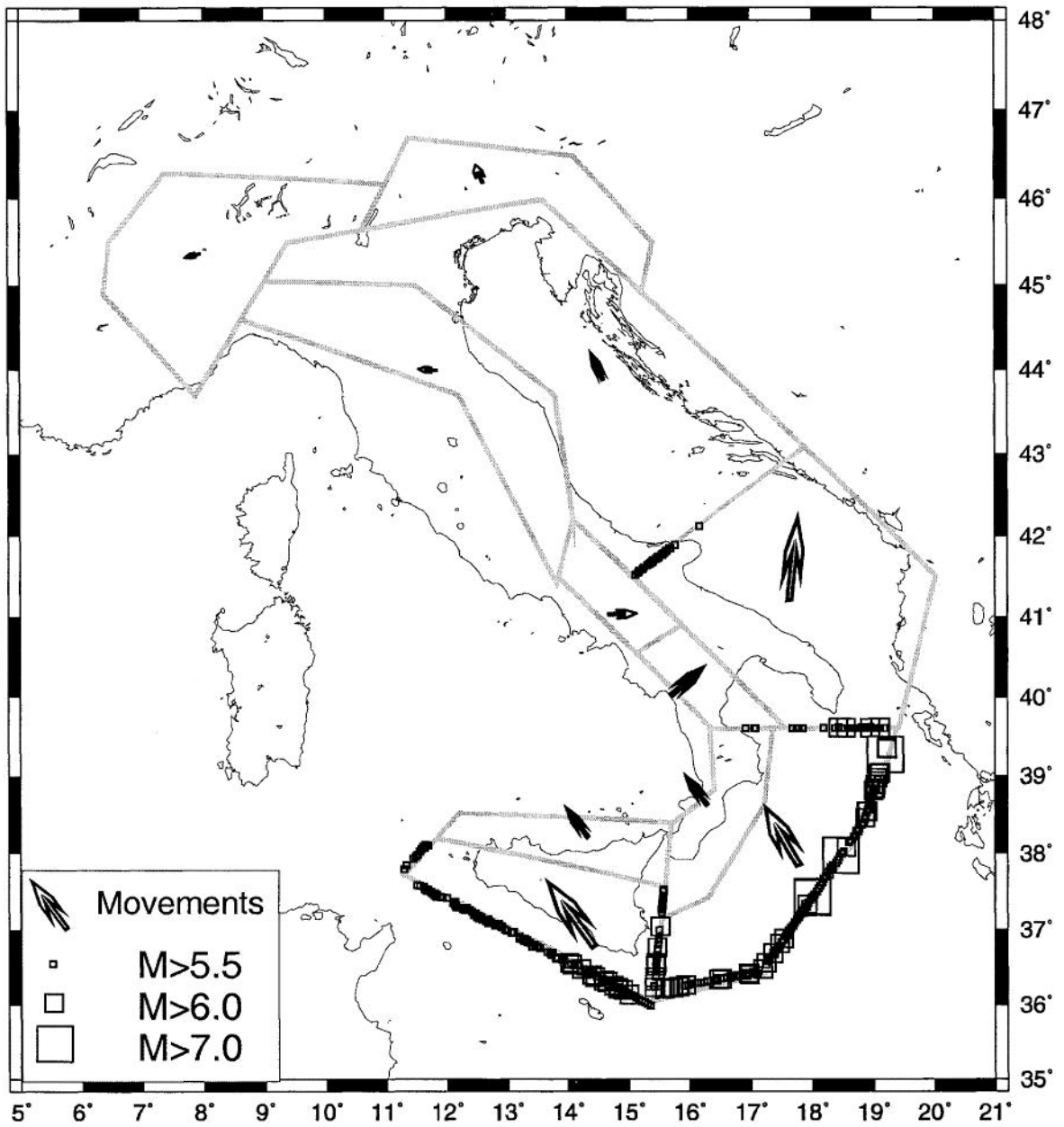


Figure 6



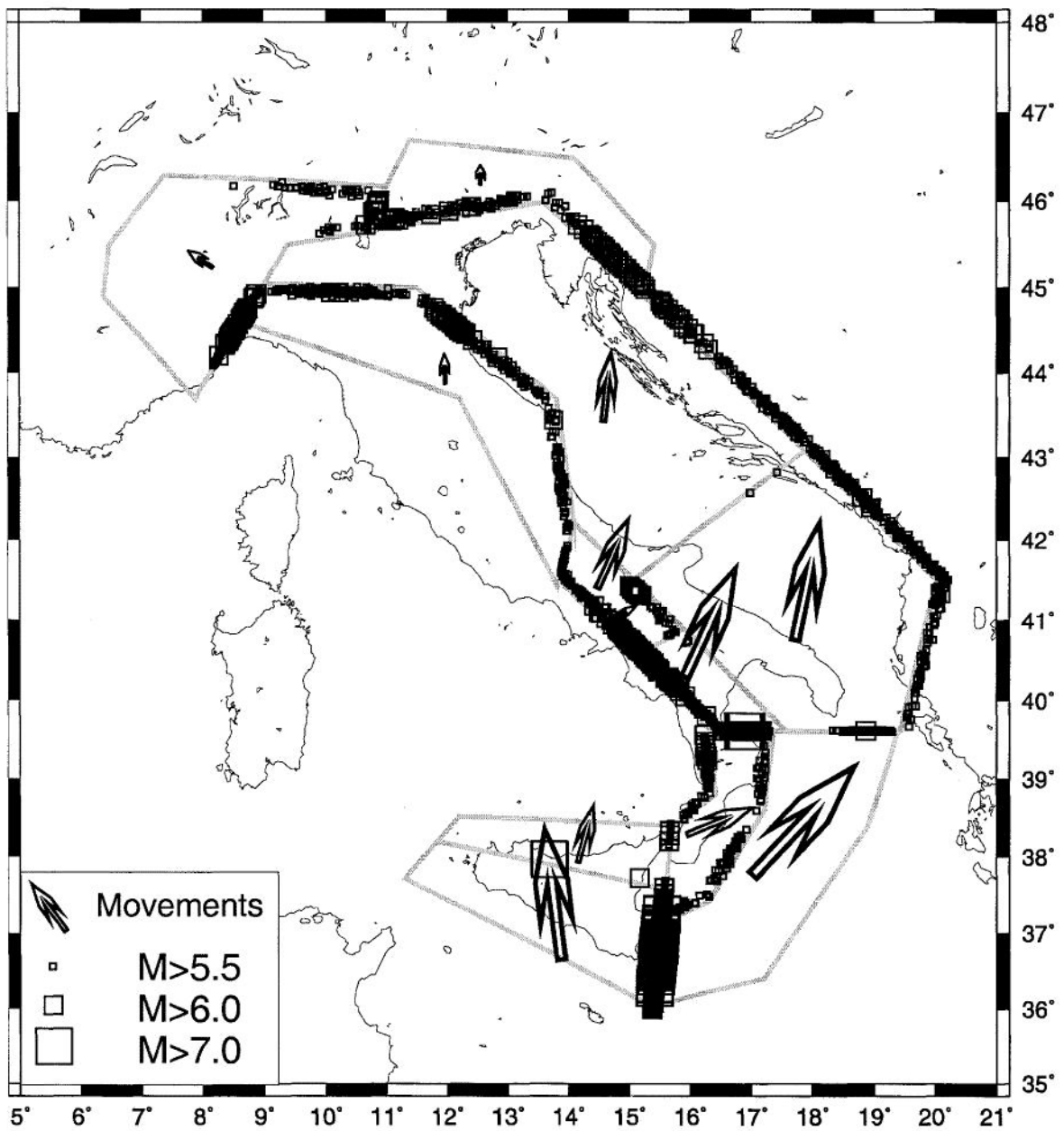
Synthetic seismicity and movements: experiment 1

Figure 7



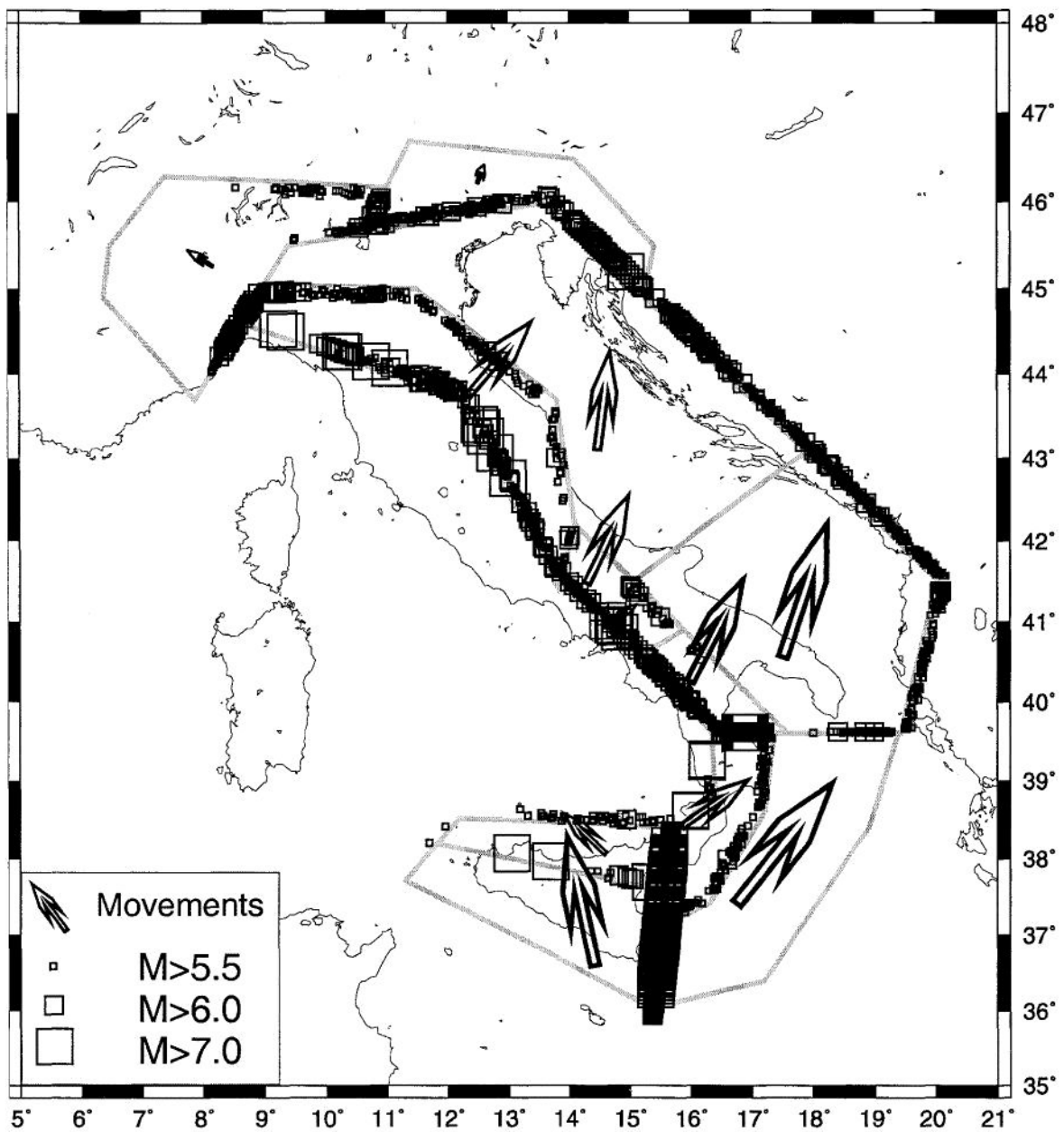
Synthetic seismicity and movements: experiment 2

Figure 8



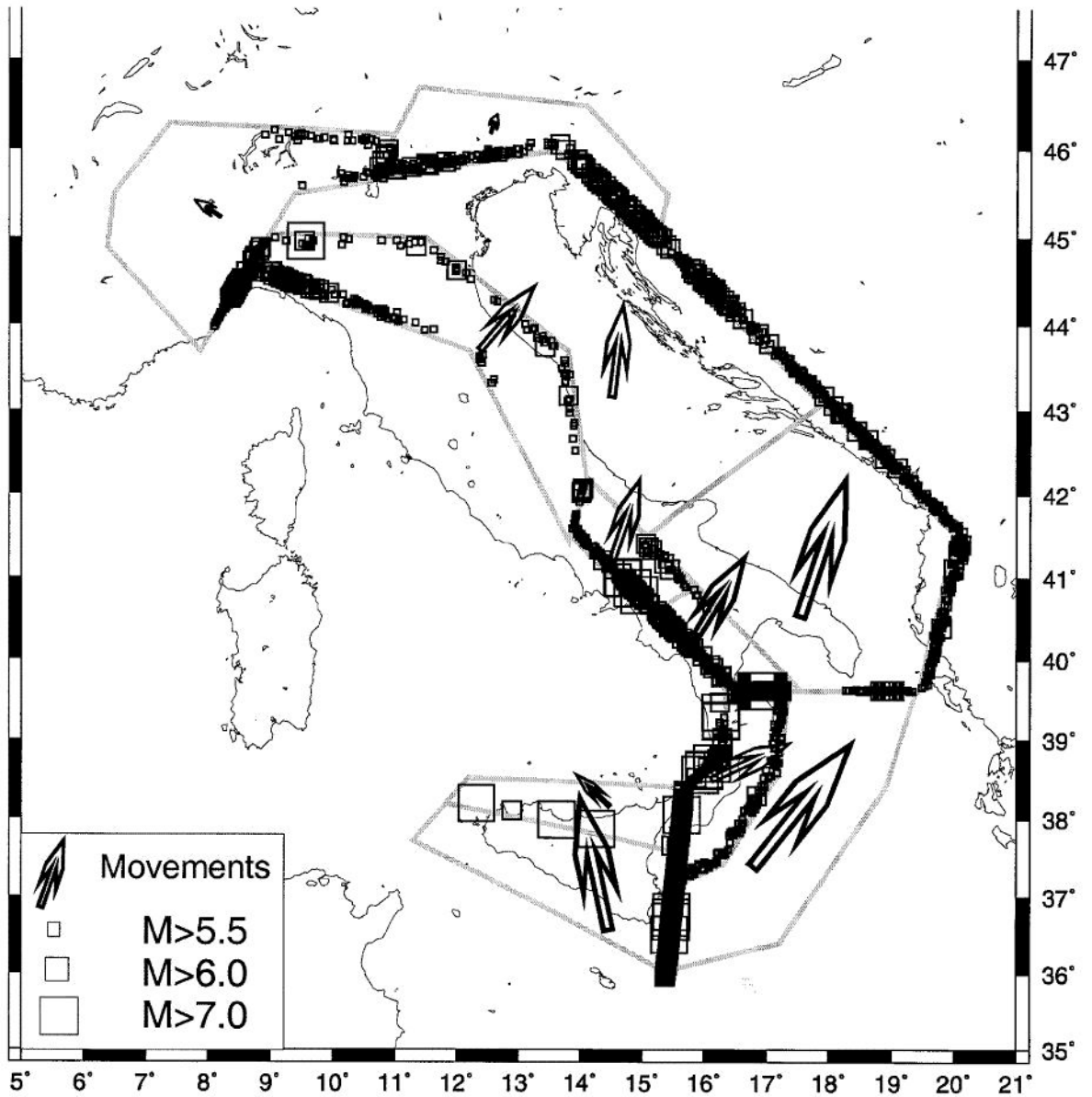
Synthetic seismicity and movements: experiment 3

Figure 9



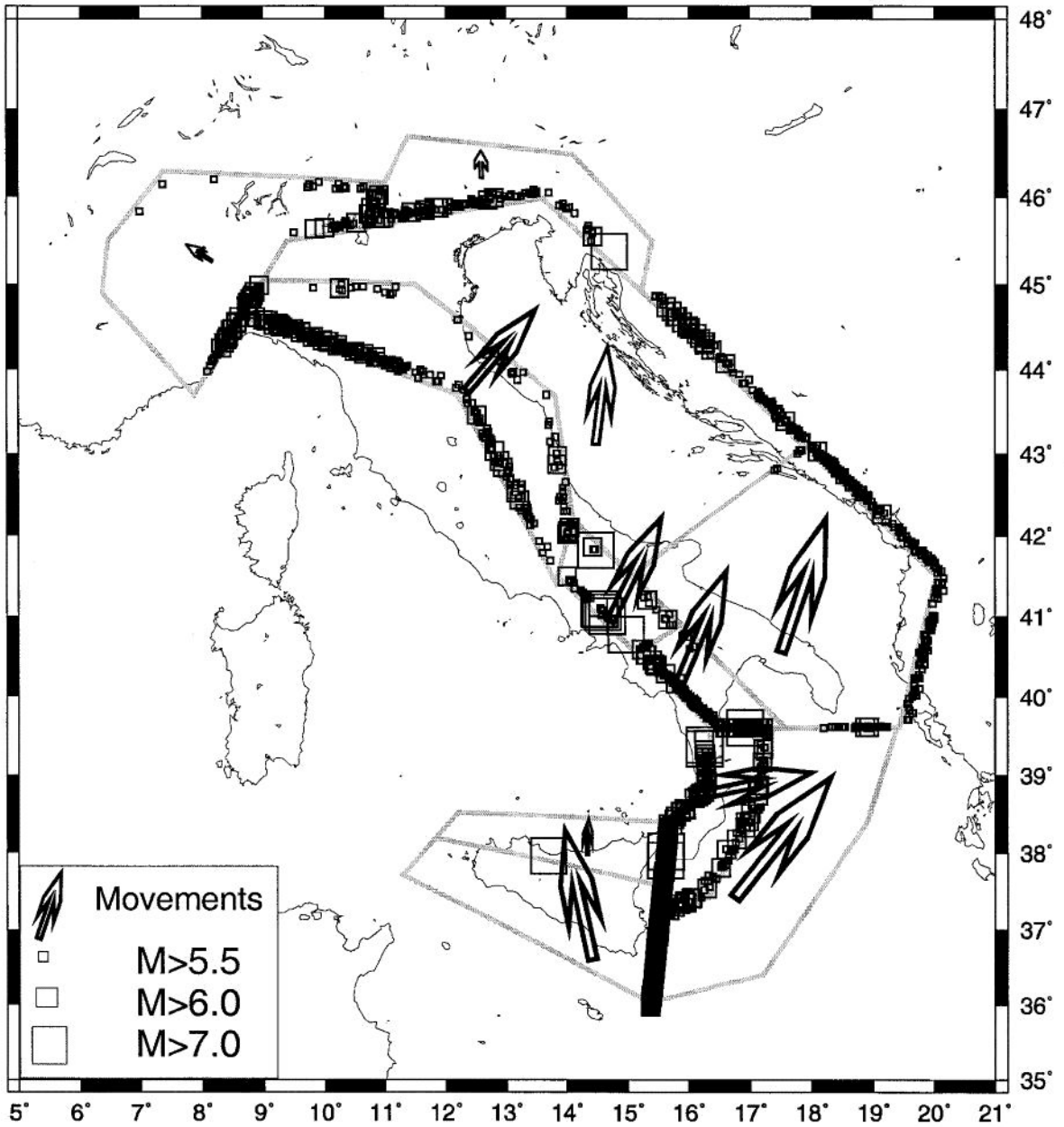
Synthetic seismicity and movements: experiment 4

Figure 10



Synthetic seismicity and movements: experiment 5

Figure 11



Synthetic seismicity and movements: experiment 6

Figure 12

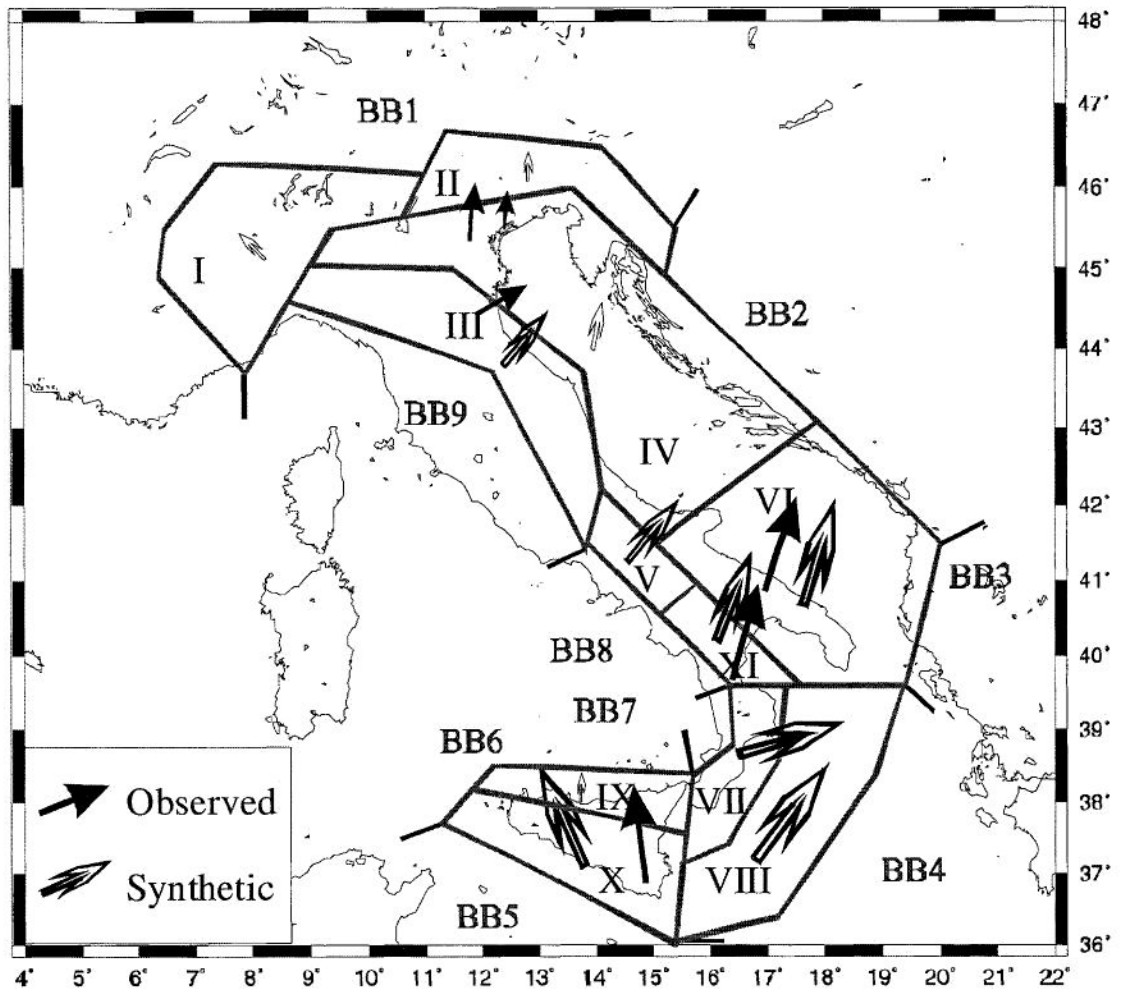


Figure 13

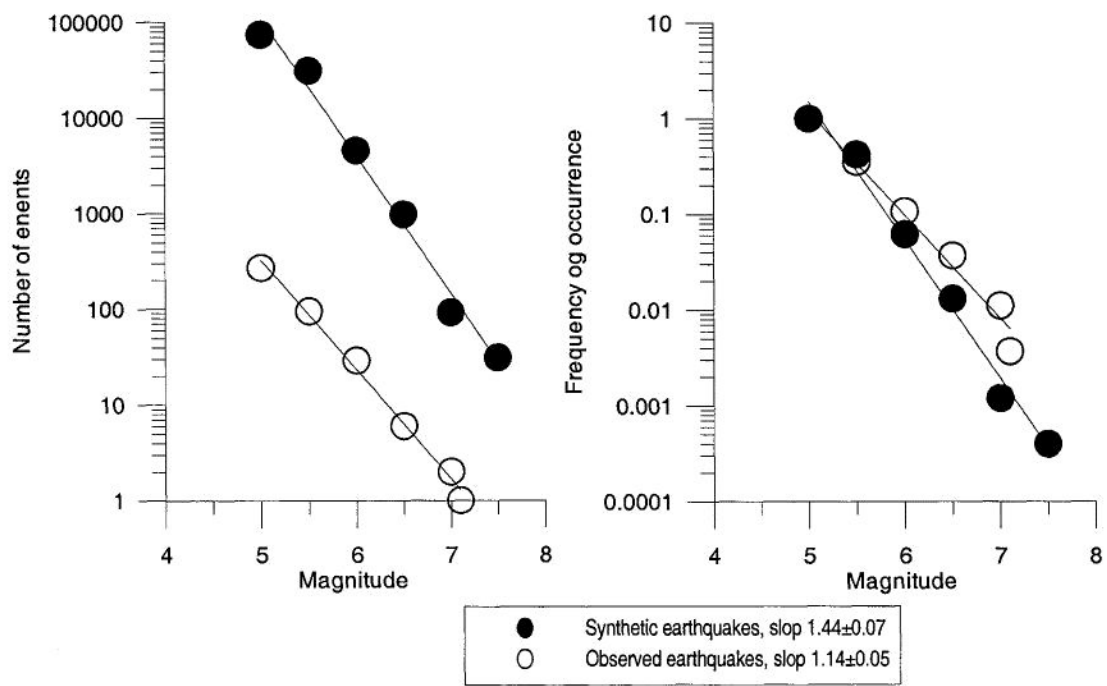


Figure 14

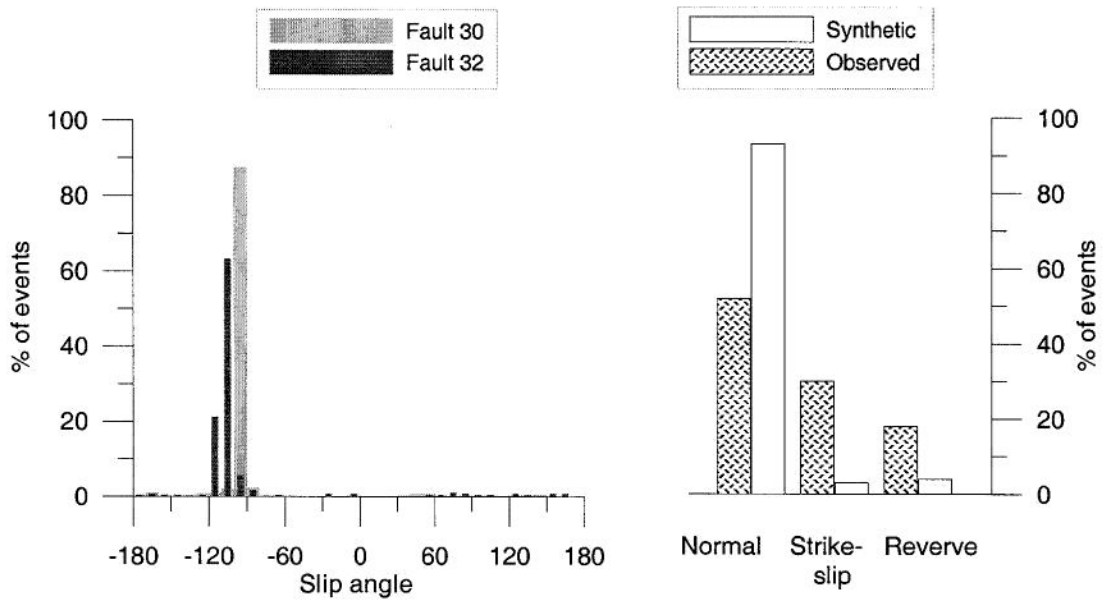


Figure 15

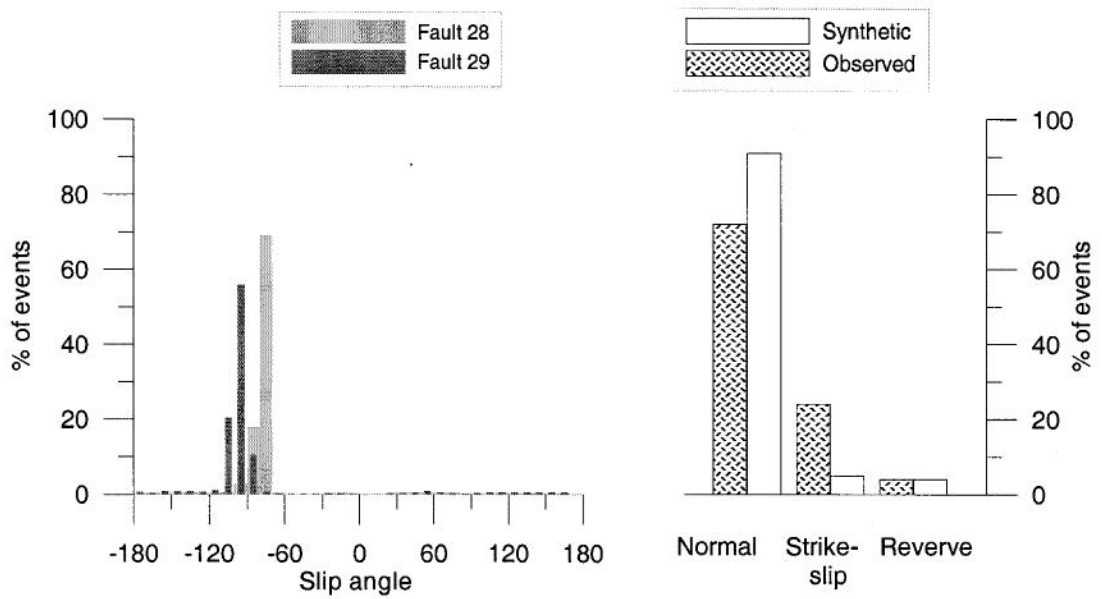


Figure 16

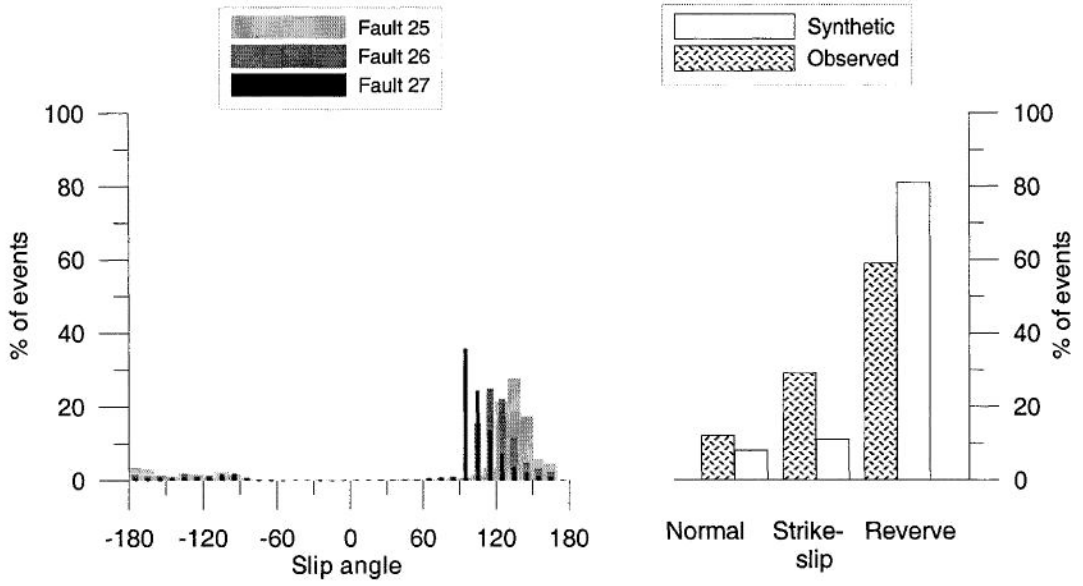


Figure 17

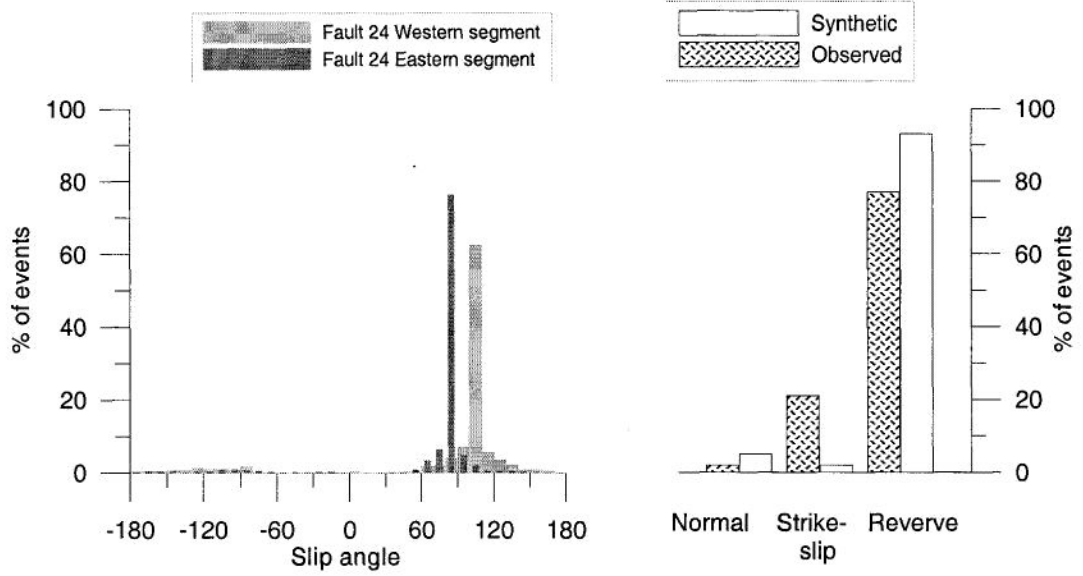


Figure 18

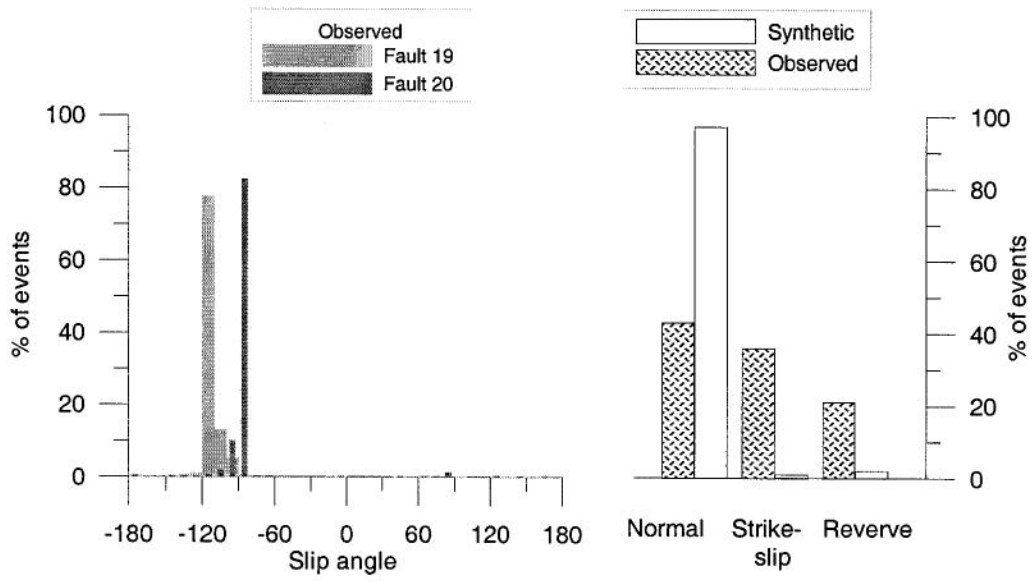


Figure 19

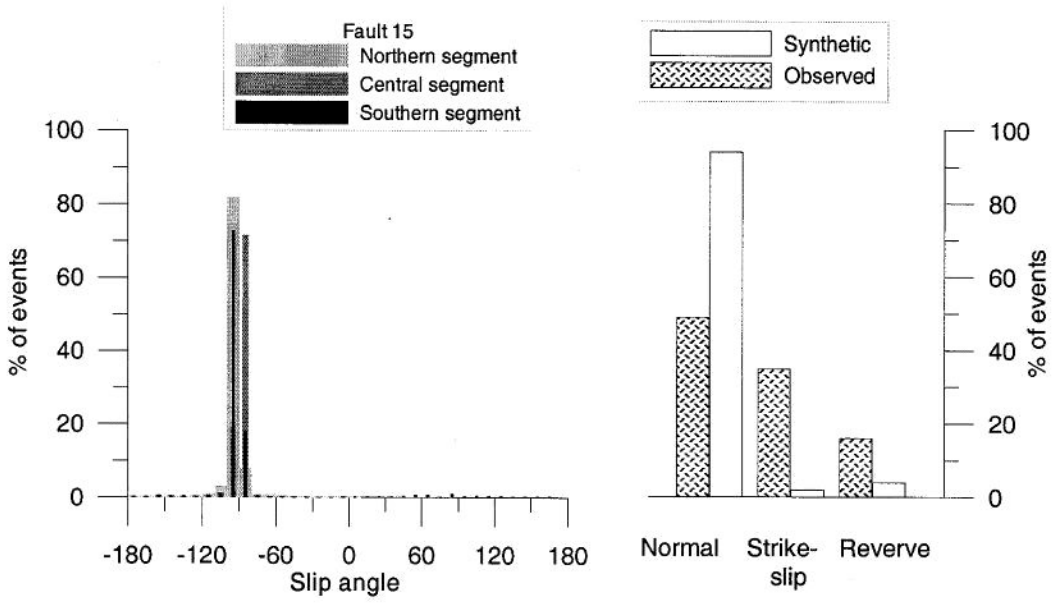


Figure 20

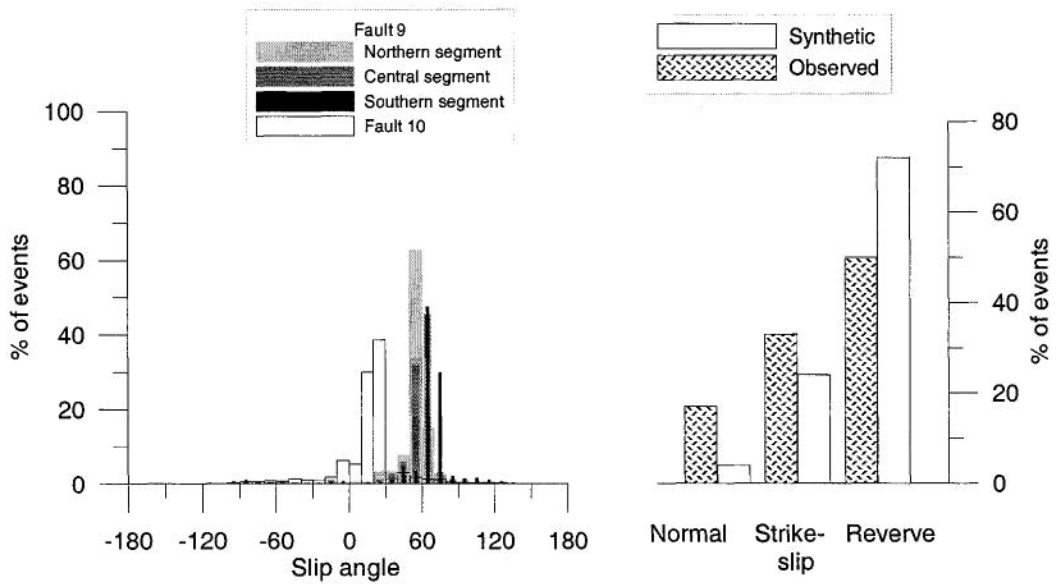


Figure 21

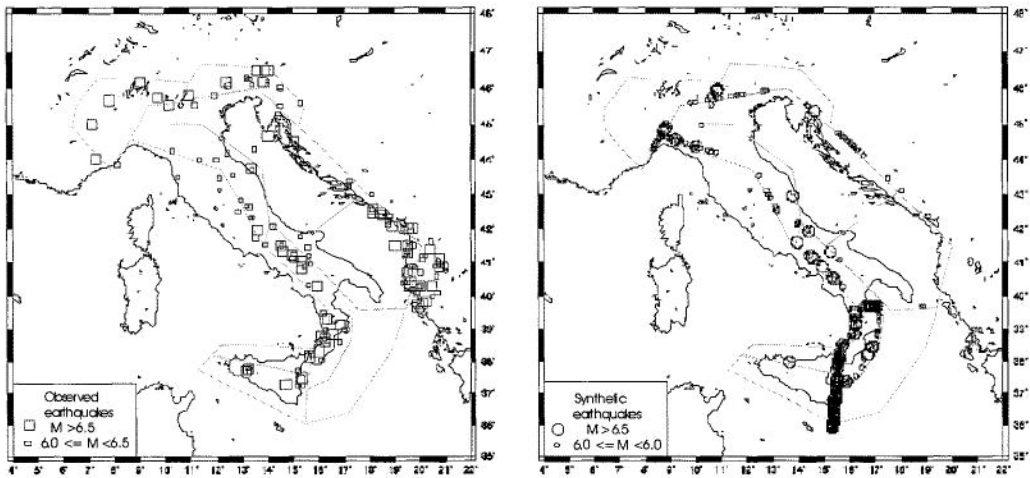


Figure 22

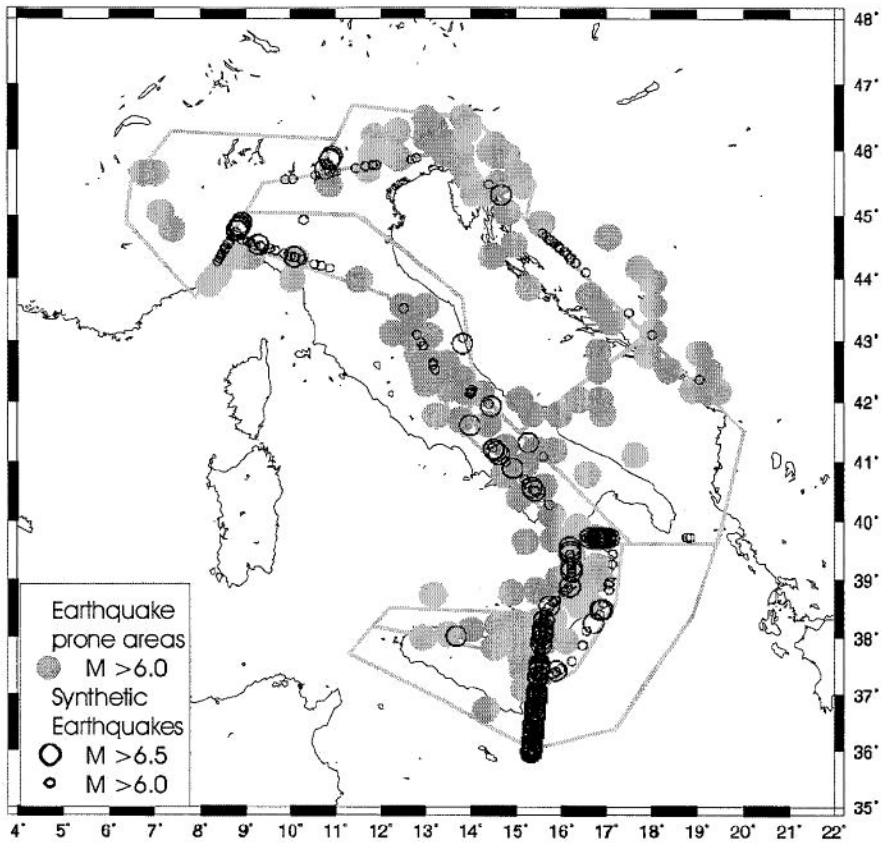


Figure 23.